Journal Pre-proofs

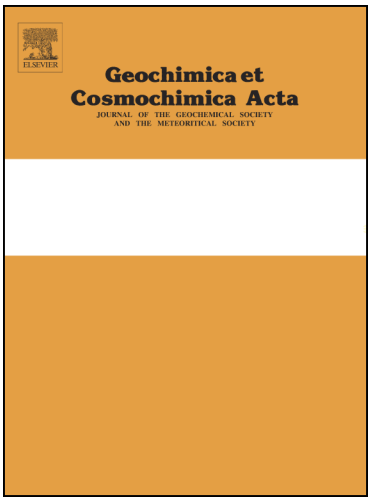

Whole-rock geochemistry and zircon O-Hf isotope compositions of ca. 2.35 Ga strongly peraluminous granites: Implications for increase in zircon δ ^{18}O values during the Paleoproterozoic

Shi-Wen Xie, Fang Wang, Claire E. Bucholz, Fu-Lai Liu, Pei-Zhi Wang, Ze-Min Bao, Dun-Yi Liu

PII: S0016-7037(22)00317-9
DOI: https://doi.org/10.1016/j.gca.2022.06.029
Reference: GCA 12693

To appear in: *Geochimica et Cosmochimica Acta*

Received Date: 30 August 2021
Revised Date: 19 June 2022
Accepted Date: 21 June 2022

Please cite this article as: Xie, S-W., Wang, F., Bucholz, C.E., Liu, F-L., Wang, P-Z., Bao, Z-M., Liu, D-Y., Whole-rock geochemistry and zircon O-Hf isotope compositions of ca. 2.35 Ga strongly peraluminous granites: Implications for increase in zircon δ ^{18}O values during the Paleoproterozoic, *Geochimica et Cosmochimica Acta* (2022), doi: https://doi.org/10.1016/j.gca.2022.06.029

Whole-rock geochemistry and zircon O-Hf isotope compositions of ca. 2.35 Ga strongly peraluminous granites: Implications for increase in zircon $\delta^{18}O$ values during the Paleoproterozoic

Shi-Wen Xie[a,b*], Fang Wang[b], Claire E. Bucholz[c], Fu-Lai Liu[b], Pei-Zhi Wang[a], Ze-Min Bao[a], Dun-Yi Liu[a]

a Beijing SHRIMP Center, Institute of Geology, Chinese Academy of Geological Sciences, Beijing 100037, China

b Key Laboratory of Deep-Earth Dynamics of Ministry of Natural Resources, Institute of Geology, Chinese Academy of Geological Sciences, Beijing 100037, China

c Division of Geological and Planetary Sciences, California Institute of Technology, 1200 E California Blvd, Pasadena, CA 91125, USA

∗ Corresponding author. E-mail address: swxie210@163.com (S.W. Xie).

ABSTRACT

Zircon oxygen isotope ratios have been used to trace the incorporation of sedimentary rocks into magmas. The dramatic increase in maximum zircon $\delta^{18}O$ values in the Paleoproterozoic observed in global databases coincides with changes in surface environments (e.g., the rise of subaerial and oxidative weathering), implying a connection between elevated zircon $\delta^{18}O$ and these changes. Zircon $\delta^{18}O$ between 2.5 to 2.2 Ga, however, is relatively under-constrained owing to limited available data in this age range. To augment data from this critical time period and understand potential causes for the elevated zircon $\delta^{18}O$ values, we report U-Pb zircon ages and $\delta^{18}O$ values

of zircon, as well as, whole-rock major and trace element geochemistry of Paleoproterozoic strongly peraluminous granites (SPGs) from the southwestern margin of the Yangtze Block (China). Our geochronological data demonstrate that these SPGs crystallized at ~2.35 Ga and that inherited zircon with ages of 2428-2721 Ma are present in these granites, indicating the source rocks of these granites were deposited, subsequently metamorphosed, and partially melted between 2.43 to 2.35 Ga. Synmagmatic zircon from samples dated in this study have $\varepsilon_{Hf}(t)$ values of −6.4 to −0.9 and high $\delta^{18}O$ values of 7.6 to 9.9‰, elevated above the maximum value observed in Archean zircon (~7‰). These granites can be divided into two groups based on whole-rock geochemistry. Both Group 1 and Group 2 granites were derived from a similar high $\delta^{18}O$, metapelitic source, but were generated by dehydration melting and hydrous melting, respectively. Our results demonstrate that the fine-grained sedimentary rocks from which the SPGs were derived had relatively high $\delta^{18}O$ (as compared to older sedimentary rocks) by 2.43-2.35 Ga. The depositional time interval of the high-$\delta^{18}O$ sedimentary sources for SPGs studied here coincides with the emergence of continental crust above sea level and the Great Oxidation Event. Supporting the findings of previous studies, the contemporaneity of our dataset with these changes in Earth's surface environments suggests that subaerial and potentially oxidative weathering contributed (at least partially) to the elevation of $\delta^{18}O$ of fine-grained sedimentary rocks. Recycling of these high-$\delta^{18}O$ sedimentary rocks into magmas contributed to the dramatic change in $\delta^{18}O$ of magmatic zircon in the earliest Paleoproterozoic. In addition, although this study is focused on a single locality, our results suggest that the abrupt

shift observed in global zircon $\delta^{18}O$ data sets likely occurred by 2.35 Ga. Last, a literature compilation of zircon $\delta^{18}O$ data from SPGs suggested that zircon $\delta^{18}O$ values may have also experienced a stepwise increase in the Neoproterozoic to Phanerozoic from 12 to 14‰. The coincidence of these increases in zircon $\delta^{18}O$ values with global oxygenation events suggests that atmospheric oxygenation may have contributed to the increase in $\delta^{18}O$ of sedimentary rocks.

Keywords: SHRIMP U-Pb dating; O-Hf isotopes; strongly peraluminous granites; elevated zircon $\delta^{18}O$; Paleoproterozoic; Yangtze Block

1. Introduction

Zircon is a robust and strongly refractory mineral with an extremely slow rate of oxygen diffusion and is therefore considered a faithful archive of the oxygen isotope composition of the magma from which it crystallized (Peck et al., 2003; Valley et al., 2003; Page et al., 2007b; Bowman et al., 2011; Bindeman et al., 2018a). Zircon in equilibrium with pristine mantle-derived magmas have a narrow range in $\delta^{18}O$ values of 5.3 ± 0.3‰ (Valley, 2003; Page et al., 2007a; Grimes et al., 2011). As zircon $\delta^{18}O$ values do not vary significantly due to magmatic differentiation (Valley et al., 2005), zircon with $\delta^{18}O$ values elevated above the "mantle" value must have crystallized from magmas which have incorporated materials that resided near the surface of the Earth (i.e., sedimentary rocks) which experienced low-temperature weathering and water-rock interactions and are characterized by high $\delta^{18}O$ values (Taylor and Sheppard, 1986). Therefore, zircon $\delta^{18}O$ is a sensitive indicator of the contributions of recycled (meta-)sedimentary rocks to magmas (e.g., Valley et al., 2005; Kemp et al., 2007; Spencer et al., 2014; Payne et al., 2015; Hopkinson et al., 2017). Consequently, variations in zircon $\delta^{18}O$ values through time can be used to trace the temporal evolution of intracrustal recycling and crust-mantle interaction. In a seminal study, Valley et al. (2005) compiled a global database of $\delta^{18}O$ in igneous zircon which demonstrated that zircon $\delta^{18}O$ values are relatively low and limited in variability (5 to 7.5‰) throughout the Archean, whereas both the range of zircon $\delta^{18}O$ values and the highest values gradually increased (up to 10‰ at ca. 1.0 Ga) during the Proterozoic (Valley et al., 2005). More recent compilations with larger databases support a dramatic increase in

the highest zircon $\delta^{18}O$ values during the post-Archean, but they show that high $\delta^{18}O$ values (above 10‰) were common in the Paleoproterozoic (Dhuime et al., 2012; Spencer et al., 2014, 2017; Payne et al., 2015). Moreover, the maximum $\delta^{18}O$ values of Paleoproterozoic and Neoproterozoic zircon are similar, implying that zircon $\delta^{18}O$ values shift abruptly between 2.5 and 2.1 Ga, but may remain relatively steady between the Paleo- to Neoproterozoic.

The causes for the increase in zircon $\delta^{18}O$ c. 2.5-2.1 Ga are debated and could be due to either enhanced recycling of supracrustal materials into magmas or an increase in the $\delta^{18}O$ of (meta-)sedimentary rocks during the early Paleoproterozoic (Valley et al., 2005; Spencer et al., 2014; Payne et al., 2015). The Paleoproterozoic increase in zircon $\delta^{18}O$ broadly coincides with the emergence of continental crust above sea level (c. 2.3-2.2 Ga; Bindeman et al., 2018b; Spencer et al., 2019; Bindeman, 2021) and the Great Oxidation Event (GOE, 2.3-2.4 Ga) (Lyons et al., 2014, and references therein), implying a connection to changes in Earth surface environments and weathering regimes (Valley et al., 2005; Spencer et al., 2019). Our understanding of causation of the increase in zircon $\delta^{18}O$ values, however, is hindered due to the relatively limited availability of zircon $\delta^{18}O$ data between 2.5-2.2 Ga. Spencer et al. (2019) augmented the detrital zircon $\delta^{18}O$ data from this critical time period and found a shift in their dataset at 2.35 Ga, but detrital zircon are difficult to provide information on the source materials and petrogenesis of their original magmatic host rocks.

Strongly peraluminous granites (SPGs) can offer an alternative archive to the detrital zircon record [SPGs have an aluminum saturation index (ASI, also referred to

as A/CNK (molar $Al_2O_3/(CaO + Na_2O + K_2O)$)) > 1.1 and contain one or more aluminous mineral (such as muscovite, garnet, or cordierite) (Sylverster, 1998).]. As SPGs are derived dominantly through the partial melting of metasedimentary rocks, they isolate the sedimentary contribution to magmas. Additionally, their zircon populations generally preserve both magmatic and inherited zircon which provides information on both magmatic isotope compositions and chemistry, as well as the age of deposition of their sedimentary source regions (akin to detrital zircon dating). SPGs have recently been the focus of study to understand how surface weathering across the Archean-Proterozoic boundary may have changed and been imprinted on the chemistry of igneous rocks (Bucholz and Spencer, 2019; Bindeman, 2021; Libemann et al., 2021a, b). For example, Liebmann et al. (2021a) documented a ~3.5‰ increase in zircon $\delta^{18}O$ of SPGs from the late Neoarchean (~2.5 Ga) to late Paleoproterozoic (~1.93 Ga). However, that study lacked significant zircon $\delta^{18}O$ data between 2.5-2.2 Ga (e.g., a single sample from the North China Craton dated at 2374 ± 48 Ma (2σ) with a sample average zircon $\delta^{18}O$ value of 7.4 ± 0.7‰, 2σ). To better understand the potential causes for the rapid increase in $\delta^{18}O$ of magmatic zircon, further studies of igneous rocks that crystallized during this time interval, and preferably characterized by a strong sedimentary component in their source regions, are required.

Recently, small volumes of SPGs with crystallization ages of ~2.35 Ga were identified in the Cuoke area, southwestern margin of the Yangtze Block (Fig. 1) (Cui et al., 2019, 2020; this study). These SPGs represent ideal targets to constrain the magmatic zircon $\delta^{18}O$ values in the earliest Paleoproterozoic and to track the isotopic

and chemical characteristics of their (meta-)sedimentary sources. Lu et al. (2021) studied three SPG samples from the Cuoke area of the Yangtze Block (South China Craton) for zircon U-Pb ages and O-Hf isotopes. The three dated granites yielded zircon U-Pb ages of 2359 ± 6 Ma, 2362 ± 5 Ma, and 2340±5 Ma. Magmatic zircon from these samples displayed sample average $\delta^{18}O$ values of 6.9 ± 0.2‰, 9.3 ± 0.2‰, 8.9 ± 0.3‰, respectively. Lu et al. (2021) interpreted this data in conjunction with existing igneous and detrital zircon data sets to indicate that continental emergence occurred between ~2.43 to 2.36 Ga. However, SPG data existing from this key locality is still limited to three samples that display variable O and Hf isotopic compositions.

Here we present a combined study of zircon U-Pb geochronology, O-Hf isotope compositions, and whole-rock geochemistry of the Cuoke SPGs. We present new zircon data for 6 samples. We then use these data to understand the source characteristics and petrogenesis of the granites, place temporal constraints on the shift in $\delta^{18}O$ of magmatic zircon in the Paleoproterozoic, and explore potential causes for the increase.

2. Geological setting and sample descriptions

The Yangtze Block is separated from the North China Craton by the Qinling-Dabie Orogen to the north, from the Cathaysia Block by the Jiangnan Fold Belt to the southeast, and is bounded by the Ailaoshan-Red River Fault to the southwest (Fig. 1A). Due to a widespread, thick Neoproterozoic and Phanerozoic cover, only small volumes of Archean to Paleoproterozoic basement rocks are exposed in its northern and southwestern margins. In the southwestern Yangtze Block, the basement rocks are

represented by metasedimentary and volcanic rocks of the Dahongshan, Dongchuan, and Hekou groups which were deposited in the late Paleoproterozoic to earliest Mesoproterozoic (1.8-1.5 Ga) and intruded by coeval granites and mafic rocks (e.g., Sun et al., 2009; Zhao et al., 2010; Chen et al., 2013; Li et al., 2013). These basement rocks are in fault contact with the late Mesoproterozoic Kunyang and Huili groups. The Dahongshan Group is the oldest lithostratigraphic sequence in the southwestern Yangtze Block (Greentree and Li, 2008) and can be subdivided from the base upwards into Laochanghe, Manganghe, Hongshan, Feiweihe, and Potou formations. The Laochanghe, Feiweihe, and Potou formations are dominated by metasedimentary rocks, including mica schist, quartz schist, marble, and carbonaceous metasedimentary rocks, whereas the Manganghe and Hongshan formations mainly consist of metavolcanic rocks, such as volcanic breccia, tuff. Apart from aforementioned metasedimentary-volcanic rocks, small volumes (about 1.4 km^2) of 2.22-2.36 Ga granites were recently identified within the Yangtze Block from the Cuoke area (Cui et al., 2019, 2020; this study).

The Cuoke area is located ~25 km northeast of Yuanjiang County along the southwestern margin of the Yangtze Block (Fig. 1). The total area of the Precambrian basement rocks in the Cuoke area is about 32 km^2 (Cui et al., 2019), which comprise granites, ultramafic-mafic intrusions, and widely exposed metasedimentary-volcanic sequences. The granites crystallized during the Paleoproterozoic and late Mesoproterozoic. The Paleoproterozoic granites occur as tectonic lenses within a roughly N-S trending ductile shear belt (Fig. 1B) and have crystallization ages of 2218-

2363 Ma (Cui et al., 2019, 2020; this study). They consist of monzogranite and granodiorite. The late Mesoproterozoic granites comprise monzogranite with minor syenogranite and crystallized at 1143-1183 Ma (Huang et al, 2021). The ultramafic-mafic intrusions include pyroxenite, gabbro, and diabase. A recent study reported crystallization ages of 2316 to 2395 Ma from four mafic samples (Liu et al., 2020). The metasedimentary-volcanic sequences, which were considered as equivalents to the Laochanghe and Manganghe formations of the Dahongshan Group, consist of quartzite, metasandstone, schist, phyllite, metaconglomerate, and metabasaltic to metaandesitic volcanic rocks (Cui et al., 2019). Geochemical results indicate that the Paleoproterozoic magmatic rocks formed during post-collisional magmatism following a ca. 2.40-2.36 Ga collisional event in the southwestern of the Yangtze Block (Cui et al., 2019, 2020; Liu et al., 2020). This collisional event was synchronous with the ca. 2.5-2.3 Ga Arrowsmith orogeny along the western flank of the Rae Craton which occurred during the assembly of the Columbia supercontinent (Wang et al., 2016; Cui et al., 2019, 2020; Liu et al., 2020).

Paleoproterozoic strongly peraluminous granites are mainly exposed along Xiaohedi River northwest of Cuoke Village (Fig. 1B). Twelve fresh samples were chosen for whole-rock major and trace elements analyses (Table S1). Among them, six representative samples were selected for zircon SHRIMP U-Pb dating (Table S2) and O-Hf isotopes analyses (Table S3). These granites are grayish-white or yellow in color and show massive or weak gneissic structures (Fig. 2). They consist dominantly of feldspar (both plagioclase and K-feldspar), quartz (80-90 vol%) and muscovite + biotite

(5-10 vol%) with accessory zircon + apatite + Fe-Ti oxides (1-5 vol%) (Fig. 3). Plagioclase and biotite are variably altered to sericite and chlorite, respectively. Compared with samples from outcrops 18YJ07, 18YJ13, and 18YJ14, samples from outcrops 18YJ15, 18YJ19, and 18YJ20 seldom contain K-feldspar grains (Fig. 3).

3. Analytical methods

3.1. Whole-rock major and trace elements

Whole-rock major and trace elements were determined at the Wuhan SampleSolution Analytical Technology Co., Ltd., Wuhan, China. X-ray fluorescence (XRF, Primus Ⅱ, Rigaku, Japan) was used to determine the major elements, whereas FeO content was determined by wet chemistry. Loss on ignition was determined gravimetrically after heating the samples in a muffle furnace to 1000°C for 2 h. Trace element concentrations were determined using an Agilent 7700e ICP-MS. The rock powder (~50 mg) was dissolved in a Teflon bomb at 190 ℃ for >24 h using a mixture HF and HNO_3 and the detailed sample-digesting procedure for ICP-MS analysis and precision and accuracy for trace elements are the same as description by Liu et al. (2008).

3.2. Zircon U-Pb dating

Zircon grains were mounted on double-sided adhesive tape, enclosed in epoxy resin, and then polished. Six samples were made two zircon mounts (18YJ07-5 and 18YJ20-1 in Mount N3552, 18YJ13-1, 18YJ13-4, 18YJ14-1, and 18YJ15-1 in Mount N3553). Cathodoluminescence (CL) imaging was conducted using a scanning electron

microscope to reveal their internal structures and to choose potential target sites for U-Pb dating analyses. U-Pb dating of zircon was performed using the SHRIMP II ion microprobe at the Beijing SHRIMP Center, CAGS, Beijing. Analytical procedures and conditions were similar to those described by Williams (1998). Mass resolution during the analytical sessions was ~5000 (1% peak height on the UO-peak of the standard). The intensity of the primary O^{-2} ion beam was 3-3.5 nA. The spot size was ~20 μm in diameter, and each site was rastered for 150-180 s prior to analysis to remove surface contamination. Reference zircon M257 (U = 840 ppm; Nasdala et al., 2008) and Plešovice ($^{206}Pb/^{238}U$ age = 337.13 Ma; Sláma et al., 2008) were used to calibrate the U abundance and U-Pb age, respectively. The M257 was analyzed only once per session. Plešovice was analyzed once every 3-4 unknown analyses. Mass analysis at each spot consisted of five scans through a sequence including Zr_2O^+, $^{204}Pb^+$, background, $^{206}Pb^+$, $^{207}Pb^+$, $^{208}Pb^+$, $^{238}U^+$, $^{232}Th^{16}O^+$, and $^{238}U^{16}O^+$ analyzed on a single electronic multiplier by cyclic stepping of the magnetic field. Data processing was carried out using the SQUID and ISOPLOT programs. Measured $^{206}Pb^+/^{238}U^+$ calibrated to the accepted $^{206}Pb/^{238}U$ ratio of the zircon standard, using a calibration curve of $\ln(^{206}Pb^+/^{238}U^+)$ vs. $\ln(UO^+/O^+)$ with a fixed slope of 2.0. Common lead correction was applied using the measured ^{204}Pb abundance. Uncertainties of individual analyses are reported at 1σ; mean weighted $^{207}Pb/^{206}Pb$ ages were calculated at 95% confidence. Reference zircon Plešovice in Mounts N3552 and N3553 yield weighted mean $^{207}Pb/^{206}Pb$ ages of 336.6 ± 2.2 Ma (MSWD = 4.4; n = 16) and 336.9 ± 2.3 Ma (MSWD = 4.4; n = 17), respectively (Table S4).

3.3. Zircon oxygen isotopes

Prior to oxygen isotope analyses, the mounts were carefully re-polished to remove the age pits. Other than 15 analyses made on undated synmagmatic domains, measurements of oxygen isotope ratios were analyzed in the dated portions of the same zircons using a multicollector SHRIMP IIe at the Beijing SHRIMP Center, CAGS. The Cs^+ primary ion beam was accelerated at 15 keV, with an intensity of ca. 13.5 nA, and focused into a spot ~25 μm in diameter on the sample surface. The separated ^{18}O and ^{16}O were simultaneously detected by dual Faraday cups with 10^{11} and 10^{10} Ω resistors. Data acquisition comprises two sets of six measurements, each with 10 s integration time, leading to total count times of ~120 s. A 150 s pre-sputter and secondary auto-tuning precede each isotopic ratio measurement. Background count rates were measured at the start of each analytical session. Instrumental mass fractionation was corrected using an in-house zircon standard Penglai with a $\delta^{18}O$ value of 5.31 ± 0.10‰ (Li et al., 2010) and measured $^{18}O/^{16}O$ ratios were normalized by using Vienna Standard Mean Ocean Water (VSMOW, $^{18}O/^{16}O$ = 0.0020052). More detailed analytical procedures and conditions are described in Ickert et al. (2008).

3.4. Zircon Lu-Hf isotopes

Hafnium isotope ratios of zircon were conducted at the Nanjing FocuMS Technology Co. Ltd., using a Nu Plasma II MC-ICP-MS with a 193 nm ArF excimer laser-ablation system. Lu-Hf isotope analyses were obtained on the same spots that were previously analyzed for O isotopes, with a spot size of 50 μm in diameter, repetition rate of 9 Hz, and laser beam energy density of 3.5 J/cm^2. Helium was applied

as carrier gas to efficiently transport aerosol out of the ablation cell and was mixed with argon before entering the ICP torch. Each measurement consisted of 20 s of acquisition of the background signal followed by 40 s of ablation signal acquisition. Masses ^{172}Yb, ^{173}Yb, ^{175}Lu, ^{176}Hf+Yb+Lu, ^{177}Hf, ^{178}Hf, ^{179}Hf and ^{180}Hf were measured simultaneously. Standard zircon GJ-1 was used as an external standard, and standard zircon 91500, Plešovice, Mud Tank, Penglai were analyzed as unknows. We applied the directly obtained mass bias of Yb (β_{Yb}) value from the zircon sample itself in real-time in this study. The ^{179}Hf/^{177}Hf ratio of 0.7325 was used to calculate the mass biases of Hf (β_{Hf}). Interferences of ^{176}Yb and ^{176}Lu on ^{176}Hf were removed from 176 mass signal using ^{176}Yb/^{172}Yb = 0.5887 and ^{176}Lu/^{175}Lu = 0.02655 (Vervoort et al., 2004). We used the mass bias of Yb (β_{Yb}) to calculate the mass fractionation of Lu because of their similar physicochemical properties.

Standard zircon yield ^{176}Hf/^{177}Hf ratios of 0.282010 ± 0.000006 (2σ, MSWD =0.46, n = 15; for GJ-1), 0.282309 ± 0.000008 (2σ, MSWD = 0.47, n = 9; for 91500), 0.282481 ± 0.000005 (2σ, MSWD = 0.39, n = 9; for Plešovice), 0.282514 ± 0.000007 (2σ, MSWD = 0.43, n = 8; for Mud Tank) and 0.282908 ± 0.000009 (2σ, MSWD =0.23, n = 8; for Penglai), consistent with the recommended values within analytical uncertainty (Table S5). A decay constant for ^{176}Lu of 1.867×10^{-11} a^{-1} (Söderlund et al., 2004), and the present-day chondritic ratios of ^{176}Hf/^{177}Hf = 0.282772 and ^{176}Lu/^{177}Hf = 0.0332 (Blichert-Toft and Albarède, 1997) were adopted to calculate $\varepsilon_{Hf}(t)$ values. Two-stage Hf model ages (t_{DM2}) were calculated by reference to depleted mantle with a present-day ^{176}Hf/^{177}Hf ratio of 0.28325 and ^{176}Lu/^{177}Hf ratio of 0.0384 (Griffin et al., 2000)

and assuming a mean $^{176}Lu/^{177}Hf$ value of 0.015 for the average continental crust (Griffin et al., 2002).

4. Results

4.1. Whole-rock geochemistry

Major and trace element compositions are given in Table S1. The 12 granite samples can be divided into two groups based on their geochemical compositions (Fig. 4). Group 1 has relatively high SiO_2 (70.14-73.17 wt.%) and K_2O (2.12-3.34 wt.%), but low Al_2O_3 (13.54-14.92 wt.%), CaO (0.41-0.69 wt.%), Na_2O (3.05-3.73 wt.%), and Na_2O/K_2O ratios (0.96-1.73). These samples are strongly peraluminous with A/CNK (molar $Al_2O_3/(CaO + Na_2O + K_2O)$) ranging from 1.42 to 1.49 (Fig. 4A). In contrast, Group 2 has relatively low SiO_2 (63.40-70.52 wt.%) and K_2O (0.87-2.86 wt.%), but high Al_2O_3 (14.39-16.29 wt.%), CaO (0.82-2.05 wt.%), Na_2O (3.28-5.18 wt.%), and Na_2O/K_2O ratios (1.15-5.97). These samples are also strongly peraluminous, but their A/CNK values (1.20-1.32) are less than those of Group 1 (Fig. 4A). Although on average Group 1 samples have lower Sr concentrations and more pronounced negative Eu anomalies as compared with Group 2, their REE and trace element patterns are similar (Fig. 5). Both Group 1 and Group 2 display fractionated REE patterns ($(La/Yb)_n$ = 8.7-38.6) and negative Eu anomalies (Eu/Eu* = 0.47-0.96; Fig. 5A). On a primitive mantle-normalized spider diagram, all samples have positive Rb, Ba, Th and Pb anomalies, and are depleted in Nb and Sr (Fig. 5B).

4.2. Geochronology

The SHRIMP zircon U-Pb dating results of six samples are presented in Table S2.

4.2.1 Sample 18YJ07-5

Zircon grains are mostly prismatic or broken prismatic fragments. Grains are 100-200 μm in length and show oscillatory zoning in cathodoluminescence (CL) images (Fig. 6A). Sixteen analyses were made on 16 grains. One (spot 16.1) gives a relatively old concordant $^{207}Pb/^{206}Pb$ age of 2667 ± 5 Ma. The others have U contents of 216-1122 ppm and Th/U ratios of 0.19-0.46 (Table S2). Apart from three analyses showing strong lead loss, the remainder yield a weighted mean $^{207}Pb/^{206}Pb$ age of 2348 ± 5 Ma (MSWD = 0.86; Fig. 7A).

4.2.2 Sample 18YJ13-1

Zircon grains are stubby to elongate in shape and range from 100 to 200 μm in length and show oscillatory zoning in CL images (Fig. 6B). Thirteen analyses have U contents ranging from 274 to 827 ppm, with Th/U ratios of 0.14-0.35 (Table S2). These analyses yield a weighted mean $^{207}Pb/^{206}Pb$ age of 2350 ± 4 Ma (MSWD = 0.49; Fig. 7B).

4.2.3 Sample 18YJ13-4

Zircon grains are stubby or elongate in shape and range from 80 to 200 μm in length. They show complex structures in CL images. Most grains are gray with oscillatory zoning, and some are truncated by dark gray to black rims (such as, grains 3 and 4 in Fig. 6C). Weakly oscillatory zoned or homogenous bright cores were preserved in ~10% of zircon grains (e.g., grains 15 and 16 in Fig. 6C). Twenty-one analyses were made on nineteen crystals. Four analyses on cores have U contents

ranging from 119 to 261 ppm, with high Th/U ratios of 0.52-1.04, and yield concordant $^{207}Pb/^{206}Pb$ ages ranging from 2538 to 2721 Ma (Table S2; Fig. 7C). Fifteen analyses on gray domains with oscillatory zoning have U contents of 170-3017 ppm (twelve of them lower than 1000 ppm) and Th/U ratios of 0.03-0.41. Eleven of these with U contents of 170-1279 ppm plot on or near concordia, yielding a weighted mean $^{207}Pb/^{206}Pb$ age of 2347 ± 4 Ma (MSWD = 0.37; Fig. 7C). Two analyses (spots 2.2, 4.2) on dark gray rims have high U contents (1245-1645 ppm) and low identical Th/U ratios (0.02). They yield $^{207}Pb/^{206}Pb$ ages ranging from 2284 to 2296 Ma, while they both show lead loss (Fig. 7C).

4.2.4 Sample 18YJ14-1

Zircon grains are euhedral and prismatic in shape and range from 60 to 200 μm in length and display oscillatory zoning in CL images (Fig. 6D). Fourteen analyses were made on 14 grains. One analysis (spot 1.1) gives a relatively old $^{207}Pb/^{206}Pb$ age of 2429 ± 9 Ma and another analysis (spot 3.1) shows strong lead loss (Fig. 7D). The other analyses have U contents ranging from 289 to 1285 ppm, with high Th/U ratios of 0.15-0.42 (Table S2), and yield a weighted mean $^{207}Pb/^{206}Pb$ age of 2352 ± 4 Ma (MSWD = 1.09; Fig. 7D).

4.2.5 Sample 18YJ15-1

Zircon grains are stubby to elongate prisms in shape ranging from 80 to 200 μm in length. In CL images, they commonly show oscillatory zoning, while several grains contain unzoned cores (Fig. 6E). Two analyses (spots 15.1, 16.1) made on cores have U contents of 39-237 ppm and Th/U ratios of 0.48-0.87. They yield $^{207}Pb/^{206}Pb$ ages

ranging from 2428 to 2689 Ma (Fig. 6E). Fourteen analyses made on oscillatory zoned domains have U contents of 205-1030 ppm and Th/U ratios of 0.11-0.33 (Table S2). Excluding spot 9.1 showing lead loss, the remaining analyses yield a weighted mean $^{207}Pb/^{206}Pb$ age of 2347 ± 5 Ma (MSWD = 0.72; Fig. 7E).

4.2.6 Sample 18YJ20-1

Zircon grains are mostly prismatic or broken prismatic fragments and 50-150 μm in length. In CL images most zircon crystals show clear oscillatory zoning (Fig. 6F). Twelve analyses on magmatic domains have U contents of 367-1143 ppm and Th/U ratios of 0.08-0.54 (Table S2). All analyses plot on or near concordia and yield a weighted mean $^{207}Pb/^{206}Pb$ age of 2347 ± 3 Ma (MSWD = 0.88; Fig. 7F).

4.3. Zircon O-Hf isotope analyses

In-situ zircon O-Hf isotope compositions of six dated samples are presented in Table S3 and Supplementary Material A. A total of seven analyses on inherited zircon cores from these samples have variable $\varepsilon_{Hf}(t)$ and $\delta^{18}O$ values. They have $\varepsilon_{Hf}(t)$ values of −10.6 to +4.4, corresponding to two-stage Hf model ages (T_{DM2}) of 2.88 to 3.67 Ga (Fig. 8A). Their $\delta^{18}O$ values range from 5.6 to 8.5‰ (Fig. 8B). Synmagmatic zircon grains in Group 1 samples (18YJ07-5, 18YJ13-1, 18YJ13-4, 18YJ14-1) exhibit similar Hf isotope compositions with $\varepsilon_{Hf}(t)$ values and T_{DM2} ages varying between −6.4 to −0.9 and 2.94 to 3.27 Ga, respectively (Fig. 8A). In this group, six analyses on discordant synmagmatic grains with discordance (disc.) ranging from 11 to 32% show relatively low $\delta^{18}O$ values of 7.1 to 8.4‰, whereas the other synmagmatic zircon plotting on or near concordant (9%>disc.>−5%, and 96% of them with disc. ranging from −5% to 5%)

have high $\delta^{18}O$ values ranging from 7.6 to 9.9‰ (Figs. 8B and 9). All synmagmatic zircon grains from Group 2 samples (18YJ15-1 and 18YJ20-1) are concordant (disc. ranging from −4% to 6%) and have homogeneous $\varepsilon_{Hf}(t)$ values of −2.1 to −4.7, corresponding to t_{DM2} ages of 3.01 to 3.17 Ga (Fig. 8A). Their $\delta^{18}O$ values range from 8.0 to 9.8‰ (Figs. 8B and 9).

As described above, six synmagmatic zircon grains from Group 1 samples have discordant U-Pb ages, but there is no significant correlation between measured $^{176}Hf/^{177}Hf$ ratios and degree of discordance (Table S3). This suggests that the Hf isotope compositions of zircon are not significantly changed by Pb loss events (Fig. 8A). However, $\delta^{18}O$ values of discordant zircon grains are on average less than those of concordant zircon grains (by ~1.6‰). As discordant grains are often depleted in ^{18}O, likely due to destruction of the zircon lattice during metamictization (Booth et al., 2005) and interaction of radiation-damaged zircon with meteoric water (Liebmann et al., 2021c), discordant zircon yielding low $\delta^{18}O$ values are excluded from the following discussion.

5. Discussion

5.1. Paleoproterozoic granites in the Cuoke area

In previous studies, several Paleoproterozoic granite outcrops were identified in the Cuoke area, north of Yuanjiang County, including strongly peraluminous granites (yellow stars in Fig. 1B), a biotite plagiogranite (MJC03), and a ferroan granite (CK01) (blue stars in Fig. 1B). These granites were emplaced at 2340-2363 Ma, 2336 Ma, and

2218 Ma, respectively (Cui et al., 2019, 2020; Lu et al., 2021). Synmagmatic zircon grains from the six SPG samples dated here commonly show oscillatory zoning in CL images and yield weighted mean $^{207}Pb/^{206}Pb$ ages ranging from 2347 to 2352 Ma (Fig. 7), which are interpreted as the crystallization ages of these granites. The results are consistent with previously published ages of Cuoke SPGs (2340-2363 Ma; Cui et al., 2019, 2020; Lu et al. 2021). Other than SPG samples (CK19-51~57) collected from the same location as CK19-52 (see Fig. 1B), the SPGs analyzed in previous works are distributed along Xiaohedi River (Fig. 1B) and share similar geochemical and isotope characteristics with our Group 1 samples (Cui et al., 2019, 2020; Lu et al. 2021) (Figs. 4, 7, 8). As shown in Fig. 1B, Group 2 granites (from outcrops 18YJ15, 18YJ19, and 18YJ20) are spatially distributed to the south of the Group 1 granites (from outcrops 18YJ07, 18YJ13, 18YJ14, CK02, CK03, CK13, CK14, CK19-74, and CK19-84) (Fig. 1B).

5.2. Petrogenesis and source characteristics

5.2.1 Source lithologies

In this study, we focused on SPGs from along the Xiaohedi River. As described above, Cuoke SPGs samples are fresh and the majority of them are undeformed. The chemical index of alteration (CIA) values of our two groups Cuoke SPGs fall in narrow ranges of 59-60 for Group 1 and of 54-57 for Group 2. These results imply major element compositions of the samples were not significantly modified by alteration, weathering. Both Group 1 and Group 2 granites are strongly peraluminous (A/CNK = 1.20-1.49) and have high zircon $\delta^{18}O$ values of 7.6-9.9‰, equivalent to whole-rock

values of 9.5-11.7‰ calculated using the method of Bucholz et al. (2017). They contain 2.7-5.2% CIPW normative corundum and minor muscovite suggesting that the strongly peraluminous granites in the Cuoke area are derived through the partial melting of metasedimentary rocks.

Vapor-absent melting experiments indicate that CaO/Na_2O ratios of SPGs are dominantly controlled by the plagioclase/clay ratios of the source with granites derived from partial melting of metapelites generally having lower CaO/Na_2O ratios (< 0.3) than those derived from partial melting of metapsammites (> 0.3) (Sylvester, 1998, and references therein). In addition, Al_2O_3/TiO_2 ratios of SPGs have been used as an indicator of the temperature of melting and involvement of biotite versus muscovite in the partial melting process. Group 1 granites have low Al_2O_3/TiO_2 (43.4-68.7) and CaO/Na_2O (0.12-0.19) ratios (Fig. 4B), indicative of their derivation from partial melting of metapelitic sources at relatively high temperature. This is also supported by their low molar $Al_2O_3/(MgO + FeO_T)$ and molar $CaO/(MgO + FeO_T)$ ratios (Fig. 4D).

Group 2 granites exhibit a relatively wide range of CaO/Na_2O ratios of 0.16-0.48 (Fig. 4B). SPGs with high CaO/Na_2O ratios can be derived from melting of plagioclase-rich psammitic sources or by mixing a pelite-derived melt with mafic magmas (Fig. 4B) (Sylvester, 1998). However, Group 2 granites plot in or near the field of partial melts from metapelitic sources in Fig. 4D and no correlation observed between their MgO contents and CaO/Na_2O (Fig. 4E). These observations do not support the above explanations.

Alternatively, CaO/Na_2O ratios of SPGs are also affected by the presence or

absence of hydrous fluids during partial melting. As the activity of water increases, the melting point of plagioclase (particularly the anorthite component) decreases, which lead to consumption of more plagioclase and an increase in CaO/Na_2O ratios in the derivative melt (Holtz and Johannes, 1991; Sylvester, 1998). Further, owing to the enhanced participation of plagioclase in melting process, melts produced by fluid-present melting have high Sr contents and low Rb/Sr ratios. Additionally, the proportion of normative Ab, An, and Or in granitic melts is strongly controlled by water activity during partial melting (Fig. 4C) (Pichavant et al., 1992; Patiño Douce, 1996; Becker et al., 1998; Weinberg and Hasalová, 2015). When excess water is present during partial melting, melts become richer in An and Ab, but poorer in Or. Consequently, high water activities produce more tonalitic to trondhjemitic melts in contrast to granitic melts generated by dehydration melting (Fig. 4C) (Pichavant et al., 1992; Patiño Douce and Harris, 1998; Castro, 2013; Weinberg and Hasalová, 2015).

In contrast to Group 1 granites, Group 2 granites are rich in An and mainly plot in the field of H_2O-present melting of metapelites (Fig. 4C). Moreover, Group 2 granites have higher Sr contents and lower Rb/Sr ratios (Fig. 4F). These observations and the discussion in the previous paragraph suggest that water-present melting of metapelitic sources produced Group 2 granites and led to their high CaO/Na_2O ratios and lower Rb/Sr ratios. In combination with nearly identical Hf isotope compositions of Group 1 and Group 2 granites (Fig. 6A), we propose that they originated from similar metasedimentary sources, but were generated by dehydration melting and hydrous melting, respectively. Compared with dehydration melting, introduction of water with

oxygen isotopes different to that of the melt source has been shown to result in a decrease in $\delta^{18}O$ of the anatectic melt (Weinberg and Hasalová, 2015, and references therein). Although $\delta^{18}O$ values of Group 1 and Group 2 fall in a similar range, Group 2 granites are more ^{18}O-depleted on average (8.5-9.0 ‰ for Group 2, whereas 8.9-9.2‰ for Group 1; Fig. 9), which implies the influx of water with lower $\delta^{18}O$ than that of their sedimentary source.

In previous studies, zircon O-Hf isotopes revealed that some granites characterized as "S-type" were not produced solely through the partial melting of metasedimentary rocks, but also had a component of mantle-derived melt (Kemp et al., 2007; Appleby et al., 2010). Because magmas from the depleted mantle have relatively high $^{177}Hf/^{176}Hf$ ratios and relatively low constant $\delta^{18}O$ values (5.5‰), incorporation of a mantle-derived magmatic component leads to increased $\varepsilon_{Hf}(t)$ and decreased $\delta^{18}O$ of granites. In this study, no mafic enclaves were observed in the Cuoke SPGs. Synmagmatic zircon show $\varepsilon_{Hf}(t)$ values of −6.4 to −0.9 and $\delta^{18}O$ values of 7.6 to 9.9‰, and there is no correlation between zircon $\varepsilon_{Hf}(t)$ and $\delta^{18}O$ (Fig. 9). Moreover, all synmagmatic zircon are within the range of the average crustal evolution trajectory of the inherited zircon in the $\varepsilon_{Hf}(t)$-age diagram (Fig. 8A). These results together with geochemical data indicate that the SPGs in the Cuoke area were derived from partial melting of a pure metapelitic source without contribution of mantle-derived component.

5.2.2 Depositional age of metasedimentary source

Synmagmatic zircon in our samples have negative $\varepsilon_{Hf}(t)$ values of −6.4 to −0.9, consistent with the previously published results (Cui et al., 2019, 2020; Lu et al., 2021).

Owing to the low $\varepsilon_{Hf}(t)$ values and their corresponding to old T_{DM2} ages, it has been suggested that the Cuoke SPGs were derived from melting of the Mesoarchean metapelitic rocks (Cui et al., 2020). However, the model ages only represent average crustal residence ages for the source of sedimentary rocks from which the SPGs were derived. On the other hand, there are many limitations of the model ages and T_{DM2} ages generally have no any age meaning (Payne et al., 2016). Therefore, the old T_{DM2} ages of Cuoke SPGs cannot be considered as the depositional ages of the sedimentary source rocks nor true periods of crustal growth (Dhuime et al., 2012). Using the age of the youngest inherited zircon core together with emplacement ages of SPGs is a useful method to constrain the maximum depositional age of the sedimentary rocks which were the source for the SPGs, similar to detrital zircon studies (Dickinson and Gehrels, 2009). In this study, the Cuoke SPGs contain two inherited cores (spots 18YJ14-1-1.1 and 18YJ15-1-15.1) yielding minimum ages of 2429 ± 9 Ma and 2428 ± 10 Ma, respectively. The depositional age of the sedimentary source rocks is therefore constrained between 2.35 and ~2.43 Ga. Inherited zircon cores have $^{207}Pb/^{206}Pb$ ages of 2428-2721 Ma and display variable zircon $\varepsilon_{Hf}(t)$ (−10.6 to +4.4) and $\delta^{18}O$ (5.6 to 8.5‰) values, indicating a complex provenance of the sedimentary source rocks.

5.3. Timing of Paleoproterozoic increase in zircon $\delta^{18}O$

As discussed in the introduction, previous studies have revealed secular changes in igneous zircon $\delta^{18}O$ values through time (Valley et al., 2005; Spencer et al., 2014, 2017; Payne et al., 2015). Generally, values of $\delta^{18}O$ in Archean igneous zircon are relatively low and fall in a narrow range (5 to 7.5‰). However, several recent studies

have reported high zircon $\delta^{18}O$ values in Neoarchean rocks (up to 11‰) (e.g., Wan et al., 2013; Ge et al., 2014) and such high $\delta^{18}O$ values were even found in 3.8 Ga magmatic zircon (Claesson et al., 2016). Although these findings are striking, these high-$\delta^{18}O$ zircon grains commonly display complex core-rim structures and their host rocks generally underwent high grade metamorphism. As the presence of fluids during high grade metamorphism can significantly modify zircon O isotope compositions, the elevated zircon $\delta^{18}O$ values may not represent primary magmatic compositions (Wan et al., 2013; Ge et al., 2014; Claesson et al., 2016).

In this study, several (n = 6) inherited Archean zircon cores have $\delta^{18}O$ of 5.6 to 8.5‰. Except for one analysis (spot 18YJ13-4-19.1, $\delta^{18}O$ = 8.5‰), the other analyses show $\delta^{18}O$ values ranging from 5.6 to 7.4‰, falling in the previously published range of Archean igneous zircon (Fig. 10). One early Paleoproterozoic core (spot 18YJ14-1-1.1, $^{207}Pb/^{206}Pb$ age = 2429 ± 9 Ma) yields $\delta^{18}O$ of 7.7‰. In contrast, the $\delta^{18}O$ values of synmagmatic zircon (~2.35 Ga) shift to 7.6-9.9‰ (Fig. 10). We consider these elevated $\delta^{18}O$ values to record magmatic values for the following reasons. First, synmagmatic zircon grains studied here are euhedral and prismatic in shape and display oscillatory zoning (Fig. 6). Second, except for six grains with discordant ages and relatively low $\delta^{18}O$ values, analyses on synmagmatic domains yield concordant ages and display similar Hf and O isotope compositions (Figs. 7-9). Third, basement rocks in the southwestern Yangtze Block underwent low-grade metamorphism, attaining only upper greenschist to lower amphibolite facies limiting potential modification of primary zircon $\delta^{18}O$ values (Greentree and Li, 2008; Zhao et al., 2010; Chen et al., 2013; Wang

et al., 2014). Although the Paleoproterozoic SPGs are present as tectonic lenses in a ductile shear belt (Fig. 1B), the samples have weak gneissic fabrics with the majority of the samples are undeformed (Cui et al., 2019, 2020; this study).

Our results are broadly consistent with the finding of Lu et al. (2021) who inferred a shift in magmatic zircon $\delta^{18}O$ values at ~2.36 Ga based on analysis of three SPG samples from Cuoke. Our data, however, provide tighter constraints on the depositional ages for the metasedimentary sources of the Cuoke SPGs with elevated magmatic $\delta^{18}O$ values. Interestingly, one sample (CK19-52) reported by Lu et al. (2021) displayed lower zircon $\delta^{18}O$ values (5.6 to 8.0‰) and zircon $\varepsilon_{Hf}(t)$ values (−10.9 to −3.9), suggesting potential derivation from an older (Archean) source. Zircon analyzed from this sample contained two inherited zircon with crystallization ages of ~2555 Ma, consistent with this interpretation.

Taken together with a global zircon $\delta^{18}O$ compilation and literature $\delta^{18}O$ data for SPGs, our new results support the previous findings of Lu et al. (2021) and provide robust evidence that the abrupt shift in magmatic zircon $\delta^{18}O$ occurred by 2.35 Ga (Fig. 10). In particular, literature $\delta^{18}O$ values for zircon from SPGs demonstrate and abrupt shift between ca. 2.5 Ga (maximum $\delta^{18}O$ = ~8‰ in Archean SPGs) to 9.9‰ at 2.35 Ga as recorded in the Cuoke SPGs.

5.4. Causes and implications of the Paleoproterozoic increase in zircon $\delta^{18}O$ values

As zircon $\delta^{18}O$ values are not significantly affected by fractional crystallization and $\delta^{18}O$ values of the mantle are homogeneous and constant throughout Earth history (Valley et al., 2005), the elevated zircon $\delta^{18}O$ values during the Paleoproterozoic

require either the incorporation of greater amounts of supracrustal material into magmas and/or a shift to higher $\delta^{18}O$ values of supracrustal materials (Valley et al., 2005; Spencer et al., 2014, 2019; Payne et al., 2015; Bindeman et al., 2018b; Bucholz and Spencer, 2019; Bindeman, 2021; Liebmann et al., 2021a, b). Recycling of greater volumes of supracrustal materials into magmas (e.g., through more vigorous plate tectonics and collisional orogenesis) can increase magma $\delta^{18}O$ values which will be reflected in magmatic zircon. For example, global compilations of zircon O isotope data show elevated average zircon $\delta^{18}O$ values at times of supercontinent assembly, due to a significant increase in the incorporation of sediments resulting from widespread orogenesis (Valley et al., 2005; Spencer et al., 2014). However, a change in quantity of recycled sediments may not lead to an increase in maximum $\delta^{18}O$ values through time, because occurrences of both Archean and Proterozoic SPGs derived from purely sedimentary sources exist (Bucholz and Spencer, 2019; Yang et al., 2019) and zircon $\delta^{18}O$ values in the Proterozoic are higher than the maximum $\delta^{18}O$ envelope in the Archean. This viewpoint is also supported by the lack of correlations with $\varepsilon_{Hf}(t)$ and $\delta^{18}O$ values of detrital zircon from Canadian and Australian supracrustal successions (Spencer et al., 2019).

Alternatively, assimilation of sedimentary rocks characterized by higher bulk $\delta^{18}O$ values into magmas may be responsible for the Paleoproterozoic elevation in zircon $\delta^{18}O$ values. Support for this viewpoint comes from the following two causes: (1) the differences in dominant lithologies of Archean and Proterozoic sedimentary rocks and (2) an increase in $\delta^{18}O$ values of fine-grained sedimentary rocks through time.

Generally, Archean sedimentary rocks comprise volcanogenic, immature clastic, and minor chemical sediments with relatively low $\delta^{18}O$ values, whereas Proterozoic sedimentary sequences are mature and rich in high-$\delta^{18}O$ clays and chemical sediments (e.g., Longstaffe and Schwarcz, 1977; Shieh and Schwarcz, 1978; Lowe, 1994; Veizer and Mackenzie, 2003; Valley et al., 2005). Consequently, magmas originating from partial melting of Archean and Proterozoic sedimentary rocks should have low and high $\delta^{18}O$ values, respectively, further causing a shift in $\delta^{18}O$ of magmatic zircon. However, whole rock geochemistry of Archean and Proterozoic SPGs suggests that there is no systematic difference in their source lithology, and some Archean SPGs were derived from partial melting of clay-rich (i.e. pelites) source regions (Bucholz and Spencer, 2019). If the $\delta^{18}O$ values of fine-grained sedimentary rocks did not change across the Archean-Proterozoic transition, Archean SPGs originating from clay-rich sources should have had similar zircon $\delta^{18}O$ to Proterozoic metapelite-derived SPGs, such as Cuoke SPGs studied here. However, almost no $\delta^{18}O$ values higher than 8.0‰ are present in the global compilation of O isotope data from both magmatic and detrital zircon (Fig. 10). Therefore, secular changes in dominant rock types from the Archean into the Proterozoic may have contributed to increases in $\delta^{18}O$ values of Proterozoic zircon, but it is likely not the main cause.

As the $\delta^{18}O$ values of fine-grained sedimentary rocks (i.e., shales) have increased through time (Longstaffe and Schwarcz, 1977; Land and Lynch, 1996; Payne et al., 2015; Bindeman et al., 2016, 2018b), the secular increase in magmatic zircon $\delta^{18}O$ values may arise simply from through assimilation of a sedimentary reservoir with more

elevated $\delta^{18}O$ values (Valley et al., 2005; Bucholz and Spencer, 2019; Spencer et al., 2019). Although existing datasets are relatively sparse, Archean fine-grained sedimentary rocks are characterized by lower $\delta^{18}O$ values on average than Proterozoic (non syn-glacial) ones (Longstaffe and Schwarcz, 1977; Bindeman et al., 2016, 2018b; Bindeman, 2021). Because oxygen isotopes of shales are controlled by the nature of low-temperature water-rock interactions (Savin and Epstein, 1970a, b), the abrupt increase in $\delta^{18}O$ of fine-grained sediments indicates that the style of weathering (i.e., degree, temperature, and meteoric water oxygen isotopic composition) changed since the late Archean. Recent work has demonstrated that $\Delta^{17}O$ of shales underwent a stepwise decrease (of 0.08‰) across the Archean-Proterozoic boundary and was attributed to a rise of subaerial continental masses resulting in more fractionated meteoric waters and cooler weathering conditions (Bindeman et al., 2018b). Taking into account a revised chronology for the shales in the aforementioned study, the decrease was considered to take place between 2.43 and 2.31 Ga (Spencer et al., 2019), which is coincident with the deposition of sedimentary sources for the Cuoke SPGs.

Because the metapelitic source rocks for the Cuoke SPGs were deposited between 2.43 to 2.35 Ga, and characterized by relatively elevated $\delta^{18}O$ values (as recorded in the synmagmatic zircon $\delta^{18}O$ values (7.6-9.9‰) in the granites), our findings constrain the timing of elevation of $\delta^{18}O$ values of fine-grained (meta-)sedimentary rocks to have occurred by 2.35-2.43 Ga. In contrast, Archean SPGs (crystallization ages of ~2.5-3.1 Ga) display comparatively low average whole-rock, zircon (5.0-7.8‰), and quartz $\delta^{18}O$ values (Fig. 10; Bucholz and Spencer, 2019, and references therein). Although our

study focuses on a single locality, the elevated zircon $\delta^{18}O$ values in the Cuoke SPGs indicate that an increase in $\delta^{18}O$ of metapelitic rocks occurred at least locally, and perhaps globally, by this time, consistent with inferences of recent studies (Spencer et al., 2019; Bindeman, 2021; Lu et al., 2021).

5.5 Zircon $\delta^{18}O$ values in SPGs across Earth history

To further demonstrate the utility of the zircon $\delta^{18}O$ record of SPGs, we compiled previously published zircon $\delta^{18}O$ values with ~3.1 Ga to Cenozoic crystallization ages (references given in the supplementary material B). Maximum zircon $\delta^{18}O$ values show two distinct increases (Fig. 10): (1) a massive increase of ~3-4‰ (from ~7‰ to ~10-12‰) during the Paleoproterozoic and (2) a smaller increase of ~2‰ (from ~12‰ to ~14‰) during the Paleozoic (Fig. 10). This trend is different from the maximum $\delta^{18}O$ envelope defined by Valley et al. (2005), because the maximum values presented here are only defined by zircon $\delta^{18}O$ of SPGs which are dominantly, if not wholly derived from sedimentary sources. Although Phanerozoic and Proterozoic SPGs could be derived from significantly older metasedimentary source rocks (e.g., Archean and Proterozoic source rocks for Phanerozoic SPGs), collectively they should sample younger rocks as younger sedimentary succession are generated and collisional processes move outwards from cratonal cores. Although sparsely populated (especially in the Proterozoic), the existing dataset of zircon $\delta^{18}O$ values of SPGs potentially indicate a two-step increase in $\delta^{18}O$ of sedimentary rocks through time and is consistent with the temporal evolution of maximum $\delta^{18}O$ values of shales (Bindeman et al., 2016, 2018b; Bindeman, 2021). Importantly, the secular change in $\delta^{18}O$ of sedimentary rocks

should be taken into consideration when the oxygen isotope compositions of zircon are used to trace the proportions of recycled sedimentary rocks through time (Payne et al., 2015). It is also worth noting that the first and second increases in maximum zircon $\delta^{18}O$ values of SPGs coincide with the Great Oxidation Event (GOE, 2.3-2.4 Ga) and Neoproterozoic to Paleozoic Oxygenation Event (0.4-0.8 Ga), respectively (Fig. 10). This implies that rising atmospheric oxygen levels may also play an important role in the increase of $\delta^{18}O$ of sedimentary rocks (Valley et al., 2005; Bucholz and Spencer, 2019). For example, Paleoproterozoic atmospheric oxygenation may have contributed to the rise in average $\delta^{18}O$ of shales through enhanced formation and diversification of clay minerals as a consequence of oxidative subaerial weathering (Hazen et al., 2013). Further, during and after the Neoproterozoic to Phanerozoic oxidation event, the evolution of multicellular life, including fungi and plants, would have enhanced the production of organic acids and mineral alteration to clays (Huang and Keller, 1972).

6. Conclusions

New geochemistry, together with zircon U-Pb ages and O-Hf isotope compositions of ~2.35 Ga strongly peraluminous granites from the Cuoke area (China) allow us to draw the following conclusions:

(1) Cuoke SPGs are mainly distributed along Xiaohedi River and can be divided into two groups. Group 1 and Group 2 granites share a similar metapelitic source, but were generated by dehydration melting and fluid-present melting, respectively.

(2) Synmagmatic zircon from the Cuoke SPGs have high $\delta^{18}O$ values of 7.6-9.9‰,

indicating that by 2.35 Ga, Paleoproterozoic zircon $\delta^{18}O$ values were elevated (at least locally and possibly globally) as compared to their Archean zircon.

(3) The sedimentary source rocks of the Cuoke SPGs were deposited between 2.43-2.35 Ga, coincident with the rapid decrease in $\Delta^{17}O$ values of shales. The occurrence of new styles of subaerial weathering which was caused by the emergence of continents above sea level may led to a dramatic increase in $\delta^{18}O$ of fine-grained sedimentary rocks during the Paleoproterozoic. Recycling of high $\delta^{18}O$ sedimentary rocks gave rise to the abrupt increase in zircon $\delta^{18}O$ values.

(4) A global compilation of Phanerozoic to Archean SPG zircon $\delta^{18}O$ values suggest a two-step increase in maximum $\delta^{18}O$ values of (meta-)pelitic rocks throughout Earth history. The coincidence of these increases with global oxygenation events suggests that atmospheric oxygenation may have contributed to the increase in $\delta^{18}O$ of sedimentary rocks.

Acknowledgements

We thank Christopher Spencer, Justin Payne and an anonymous reviewer for their detailed comments that helped us to improve the manuscript substantially. Editor Weidong Sun and Jeffrey G. Catalano are thanked for editorial assistance and for constructive comments. This research was supported by National Natural Science Foundation of China (grant numbers 91855206, 41772193, 42172219, 41402167), the Fund from the Key Laboratory of Deep-Earth Dynamics of Ministry of Natural Resources (grant numbers J1901-20-9, J1901-8, J1901-20-2), and the Key Scientific

and Technological Innovation Project of Shandong Province.

References

Altherr R., Holl A., Hegner E., Langer C. and Kreuzer H. (2000) High-potassium, calc-alkaline I-type plutonism in the European Variscides: northern Vosges (France) and northern Schwarzwald (Germany). *Lithos* **50**, 51–73.

Appleby S. K., Gillespie M. R., Graham C. M., Hinton R. W., Oliver G. J. and Kelly N. M. (2010) Do S-type granites commonly sample infracrustal sources? New results from an integrated O, U–Pb and Hf isotope study of zircon. *Contrib. Mineral. Petrol.* **160**, 115–132.

Barker F. (1979) Trondhjemite: definition, environment and hypotheses of origin. In *Trondhjemites, Dacites and Related Rocks* (eds. F. Barker). Elsevier, Amsterdam, pp. 1–12.

Becker A., Holtz F. and Johannes W. (1998) Liquidus temperatures and phase compositions in the system Qz-Ab-Or at 5 kbar and very low water activities. *Contrib. Mineral. Petrol.* **130**, 213–224.

Bindeman I. N. (2021) Triple oxygen isotopes in evolving continental crust, granites, and clastic sediments. *Rev. Mineral. Geochem.* **86**, 241–290.

Bindeman I., Bekker A. and Zakharov D. (2016) Oxygen isotope perspective on crustal evolution on early Earth: A record of Precambrian shales with emphasis on Paleoproterozoic glaciations and Great Oxygenation Event. *Earth Planet. Sci. Lett.* **437**, 101–113.

Bindeman I. N., Schmitt A. K., Lundstrom C. C. and Hervig R. L. (2018a) Stability of zircon and its isotopic ratios in high-temperature fluids: Long-term (4 months) isotope exchange experiment at 850°C and 50 MPa. *Front. Earth Sci.* **6**, 1–15.

Bindeman I. N., Zakharov D. O., Palandri J., Greber N. D., Dauphas N., Retallack G. J., Hofmann A., Lackey J. S. and Bekker A. (2018b) Rapid emergence of subaerial landmasses and onset of a modern hydrologic cycle 2.5 billion years ago. *Nature* **557**, 545–548.

Blichert-Toft J. and Albarède F. (1997) The Lu-Hf isotope geochemistry of chondrites and the evolution of the mantle-crust system. *Earth Planet. Sci. Lett.* **148**, 243–258.

Booth A. L., Kolodny Y., Chamberlain C. P., McWilliams M., Schmitt A. K. and Wooden J. (2005) Oxygen isotopic composition and U-Pb discordance in zircon. *Geochim. Cosmochim. Acta* **69**, 4895–4905.

Bowman J. R., Moser D. E., Valley J. W., Wooden J. L., Kita N. T. and Mazdab F. K. (2011) Zircon U-Pb isotope, $\delta^{18}O$ and trace element response to 80 my of high temperature metamorphism in the lower crust: Sluggish diffusion and new records of Archean craton formation. *Am. J. Sci.* **311**, 719–772.

Bucholz C. E., Jagoutz O., VanTongeren J. A., Setera J. and Wang Z. (2017) Oxygen isotope trajectories of crystallizing melts: Insights from modeling and the plutonic record. *Geochim. Cosmochim. Acta* **207**, 154–184.

Bucholz C. E. and Spencer C. J. (2019) Strongly Peraluminous Granites across the Archean–Proterozoic Transition. *J. Petrol.* **60**, 1299–1348.

Castro A. (2013) Tonalite-granodiorite suites as cotectic systems: A review of experimental studies with applications to granitoid petrogenesis. *Earth-Sci. Rev.* **124**, 68–95.

Chen W. T., Zhou M. F. and Zhao X. F. (2013) Late Paleoproterozoic sedimentary and mafic rocks in the Hekou area, SW China: Implication for the reconstruction of the Yangtze Block in Columbia. *Precambrian Res.* **231**, 61–77.

Claesson S., Bibikova E. V., Shumlyanskyy L., Whitehouse M. J. and Billström K. (2016) Can oxygen isotopes in magmatic zircon be modified by metamorphism? A case study from the Eoarchean Dniester-Bug Series, Ukrainian Shield. *Precambrian Res.* **273**, 1–11.

Cui X. Z., Wang J., Ren G. M., Deng Q., Sun Z. M., Ren F. and Chen F. L. (2020) Paleoproterozoic tectonic evolution of the Yangtze Block: New evidence from ca. 2.36 to 2.22 Ga magmatism and 1.96 Ga metamorphism in the Cuoke complex, SW China. *Precambrian Res.* **337**, 105525.

Cui X. Z., Wang J., Sun Z. M., Wang W., Deng Q., Ren G. M., Liao S. Y., Huang M. D., Chen F. L. and Ren F. (2019) Early Paleoproterozoic (ca. 2.36 Ga) post-collisional granitoids in Yunnan, SW China: Implications for linkage between Yangtze and Laurentia in the Columbia supercontinent. *J. Asian Earth Sci.* **169**, 308–322.

Dhuime B., Hawkesworth C. J., Cawood P. A. and Storey C. D. (2012) A change in the geodynamics of continental growth 3 billion years ago. *Science* **335**, 1334–1336.

Dickinson W. R. and Gehrels G. E. (2009) Use of U–Pb ages of detrital zircons to infer

maximum depositional ages of strata: A test against a Colorado Plateau Mesozoic database. *Earth Planet. Sci. Lett.* **288**, 115–125.

Ge R. F., Zhu W. B., Wilde S. A., Wu H. L., He J. W. and Zheng B. H. (2014) Archean magmatism and crustal evolution in the northern Tarim Craton: Insights from zircon U–Pb–Hf–O isotopes and geochemistry of ~ 2.7Ga orthogneiss and amphibolite in the Korla Complex. *Precambrian Res.* **252**, 145–165.

Greentree M. R. and Li Z.X. (2008) The oldest known rocks in south–western China: SHRIMP U–Pb magmatic crystallisation age and detrital provenance analysis of the Paleoproterozoic Dahongshan Group. *J. Asian Earth Sci.* **33**, 289–302.

Griffin W. L., Pearson N. J., Belousova E., Jackson S. E., Achterbergh E. V., O'Reilly S. Y. and Shee S. R. (2000) The Hf isotope composition of cratonic mantle: LAM-MC-ICPMS analysis of zircon megacrysts in kimberlites. *Geochim. Cosmochim. Acta* **64**, 133–147.

Griffin W. L., Wang X., Jackson S. E., Pearson N. J., O'Reilly S. Y., Xu X. and Zhou X. (2002) Zircon chemistry and magma mixing, SE China: in-situ analysis of Hf isotopes, Tonglu and Pingtan igneous complexes. *Lithos* **61**, 237–269.

Hazen R. M., Sverjensky D. A., Azzolini D., Bish D. L., Elmore S. C., Hinnov L. and Milliken R. E. (2013) Clay mineral evolution. *Am. Mineral.* **98**, 2007–2029.

Holtz F. and Johannes W. (1991) Genesis of peraluminous granites I. Experimental investigation of melt compositions at 3 and 5 kb and various H_2O activities. *J. Petrol.* **32**, 935–958.

Hopkinson T. N., Harris N. B. W., Warren C. J., Spencer C. J., Roberts N. M. W.,

Horstwood M. S. A., Parrish R. R. and Eimf (2017) The identification and significance of pure sediment-derived granites. *Earth Planet. Sci. Lett.* **467**, 57–63.

Huang M. D., Cui X. Z., Lin S. F., Chen J. B., Ren G. M., Sun Z. M., Ren F. and Xu Q. (2021) The ca. 1.18–1.14 Ga A-type granites in the southwestern Yangtze Block, South China: New evidence for late Mesoproterozoic continental rifting. *Precambrian Res.* **363**, 106358.

Huang W. H. and Keller W. D. (1972) Organic Acids as Agents of Chemical Weathering of Silicate Minerals. *Nature Phys. Sci.* **239**, 149–151.

Ickert R. B., Hiess J., Williams I. S., Holden P., Ireland T. R., Lanc P., Schram N., Foster J. J. and Clement S. W. (2008) Determining high precision, in situ, oxygen isotope ratios with a SHRIMP II: Analyses of MPI-DING silicate-glass reference materials and zircon from contrasting granites. *Chem. Geol.* **257**, 114–128.

Inger S. and Harris N. (1993) Geochemical Constraints on Leucogranite Magmatism in the Langtang Valley, Nepal Himalaya. *J. Petrol.* **34**, 345–368.

Kemp A. I. S., Hawkesworth C. J., Foster G. L., Paterson B. A., Woodhead J. D., Hergt J. M., Gray C. M. and Whitehouse M. J. (2007) Magmatic and crustal differentiation history of granitic rocks from Hf-O isotopes in zircon. *Science* **315**, 980–983.

Kump L. R. (2008) The rise of atmospheric oxygen. Nature **451**, 277–278.

Land L. S. and Leo Lynch F. (1996) $\delta^{18}O$ values of mudrocks: More evidence for an ^{18}O-buffered ocean. *Geochim. Cosmochim. Acta* **60**, 3347–3352.

Li H. K., Zhang C. L., Yao C. Y. and Xiang Z. Q. (2013) U-Pb zircon age and Hf isotope compositions of Mesoproterozoic sedimentary strata on the western margin of the Yangtze massif. *Sci. China Earth Sci.* **56**, 628–639.

Li X. H., Long W. G., Li Q. L., Liu Y., Zheng Y. F., Yang Y. H., Chamberlain K. R., Wan D. F., Guo C. H., Wang X. C. and Tao H. (2010) Penglai zircon megacrysts: A potential new working reference material for microbeam determination of Hf–O Isotopes and U–Pb age. *Geostand. Geoanal. Res.* **34**, 117–134.

Liebmann J., Spencer C. J., Kirkland C. L., E. Bucholz C., He X. F., Santosh M., Xia X. P., Martin L. and Evans N. J. (2021a) Emergence of continents above sea-level influences sediment melt composition. *Terra Nov.* **00**, 1–10.

Liebmann J., Spencer C. J., Kirkland C. L., Bucholz C. E., Xia X. P., Martin L., Kitchen N. and Shumlyanskyy L. **(**2021b) Coupling sulfur and oxygen isotope ratios in sediment melts across the Archean-Proterozoic transition. *Geochim. Cosmochim. Acta* **307**, 242–257.

Liebmann J., Spencer C. J., Kirkland C. L., Xia X. P. and Bourdet J. (2021c) Effect of water on δ18O in zircon. *Chem. Geol.* **574**, 120243.

Liu G. C., Qian X., Li J., Zi J. W., Zhao T. Y., Feng Q. L., Chen G. Y. and Hu S. B. (2020) Geochronological and Geochemical Constraints on the Petrogenesis of Early Paleoproterozoic (2.40-2.32 Ga) Nb-Enriched Mafic Rocks in Southwestern Yangtze Block and Its Tectonic Implications. *J. Earth Sci.* **31**, 35–52.

Liu Y. S., Zong K. Q., Kelemen P. B. and Gao S. (2008) Geochemistry and magmatic

history of eclogites and ultramafic rocks from the Chinese continental scientific drill hole: Subduction and ultrahigh-pressure metamorphism of lower crustal cumulates. *Chem. Geol.* **247**, 133–153.

Longstaffe F. J. and Schwarcz H. P. (1977) $^{18}O/^{16}O$ of Archean clastic metasedimentary rocks: a petrogenetic indicator for Archean gneisses? *Geochim. Cosmochim. Acta* **41**, 1303–1312.

Lowe D. R. (1994) Archean greenstone-related sedimentary rocks. In *Developments in Precambrian Geology* (eds. K. C. Condie). Elsevier, pp. 121–169.

Lu G. M., Spencer C. J., Tian Y. and Wang W. (2021) Significant increase of continental freeboard during the early Paleoproterozoic: Insights from metasediment-derived granites. *Geophys. Res. Lett.* **48**, e2021GL096049.

Lyons T. W., Reinhard C. T. and Planavsky N. J. (2014) The rise of oxygen in Earth's early ocean and atmosphere. *Nature* **506**, 307–315.

Nasdala L., Hofmeister W., Norberg N., Martinson J. M., Corfu F., Dörr W., Kamo S. L., Kennedy A. K., Kronz A., Reiners P. W., Frei D., Kosler J., Wan Y., Götze J., Häger T., Kröner A. and Valley J. W. (2008) Zircon M257 - a homogeneous natural reference material for the ion microprobe U-Pb analysis of zircon. *Geostand. Geoanal. Res.* **32**, 247–265.

Page F. Z., Fu B., Kita N. T., Fournelle J., Spicuzza M. J., Schulze D. J., Viljoen F., Basei M. A. S. and Valley J.W. (2007a) Zircons from kimberlite: New insights from oxygen isotopes, trace elements, and Ti in zircon thermometry. *Geochim. Cosmochim. Acta* **71**, 3887–3903.

Page F. Z., Ushikubo T., Kita N. T., Riciputi L. and Valley J. W. (2007b) High-precision oxygen isotope analysis of picogram samples reveals 2 μm gradients and slow diffusion in zircon. *Am. Mineral.* **92**, 1772–1775.

Partin C. A., Bekker A., Sylvester P. J., Wodicka N., Stern R. A., Chacko T. and Heaman L. M. (2014) Filling in the juvenile magmatic gap: Evidence for uninterrupted Paleoproterozoic plate tectonics. *Earth Planet. Sci. Lett.* **388**, 123–133.

Patiño Douce A. E. (1996) Effects of pressure and H_2O content on the compositions of primary crustal melts. *Trans. R. Soc. Edinburgh: Earth Sci.* **87**, 11–21.

Patiño Douce A. E. and Harris N. (1998) Experimental constraints on Himalayan anatexis. *J. Petrol.* **39**, 689–710.

Payne J. L., Hand M., Pearson N. J., Barovich K. M. and McInerney D. J. (2015) Crustal thickening and clay: Controls on O isotope variation in global magmatism and siliciclastic sedimentary rocks. *Earth Planet. Sci. Lett.* **412**, 70–76.

Payne J. L., McInerney D. J., Barovich K. M., Kirkland C. L., Pearson N. J. and Hand M. (2016) Strengths and limitations of zircon Lu-Hf and O isotopes in modelling crustal growth. *Lithos* **248-251**, 175–192.

Peck W. H., Valley J. W. and Graham C. M. (2003) Slow oxygen diffusion rates in igneous zircons from metamorphic rocks. *Am. Mineral.* **88**, 1003–1014.

Pichavant M., Holtz F. and McMillan P. F. (1992) Phase relations and compositional dependence of H_2O solubility in quartz-feldspar melts. *Chem. Geol.* **96**, 303–319.

Savin S. M. and Epstein S. (1970a) The oxygen and hydrogen isotope geochemistry of

clay minerals. *Geochim. Cosmochim. Acta* **34**, 25–42.

Savin S. M. and Epstein S. (1970b) The oyxgen and hydrogen isotope geochemistry of ocean sediments and shales. *Geochim. Cosmochim. Acta* **34**, 43–63.

Shieh Y. N. and Schwarcz H. P. (1978) The oxygen isotope composition of the surface crystalline rocks of the Canadian Shield. *Can. J. Earth Sci.* **15**, 1773–1782.

Sláma J., Košler J., Condon D. J., Crowley J. L., Gerdes A., Hanchar J. M., Horstwood M. S. A., Morris G. A., Nasdala L., Norberg N., Schaltegger U., Schoene B., Tubrett M. N. and Whitehouse M. J. (2008) Plešovice zircon — A new natural reference material for U–Pb and Hf isotopic microanalysis. *Chem. Geol.* **249**, 1–35.

Söderlund U., Patchett P. J., Vervoort J. D. and Isachsen C. E. (2004) The ^{176}Lu decay constant determined by Lu–Hf and U–Pb isotope systematics of Precambrian mafic intrusions. *Earth Planet. Sci. Lett.* **219**, 311–324.

Spencer C. J., Cawood P. A., Hawkesworth C. J., Raub T. D., Prave A. R. and Roberts N. M. (2014) Proterozoic onset of crustal reworking and collisional tectonics: Reappraisal of the zircon oxygen isotope record. *Geology* **42**, 451–454.

Spencer C. J., Partin C. A., Kirkland C. L., Raub T. D., Liebmann J. and Stern R. A. (2019) Paleoproterozoic increase in zircon δ^{18}O driven by rapid emergence of continental crust. *Geochim. Cosmochim. Acta* **257**, 16–25.

Spencer C. J., Roberts N. M. W. and Santosh M. (2017) Growth, destruction, and preservation of Earth's continental crust. *Earth-Sci. Rev.* **172**, 87–106.

Sun S. S. and McDonough W. F. (1989) Chemical and isotopic systematics of oceanic

basalts: implications for mantle composition and processes. *Geol. Soc. (Lond.) Spec. Publ.* **42**, 313–345.

Sylvester P. J. (1998) Post-collisional strongly peraluminous granites. *Lithos* **45**, 29–44.

Taylor H. P. and Sheppard S. M. F. (1986) Igneous rocks: I. Processes of isotopic fractionation and isotope systematics. In *Stable Isotopes in High Temperature Geological Processes* (eds. J. W. Valley, H. P. Taylor and J. R. O'Neil). Mineralogical Society of America, Washington, pp. 227–271.

Valley J. W. (2003) Oxygen isotopes in zircon. *Rev. Mineral. Geochem.* **53**, 343–385.

Valley J. W., Lackey J. S., Cavosie A. J., Clechenko C. C., Spicuzza M. J., Basei M. A. S., Bindeman I. N., Ferreira V. P., Sial A. N., King E. M., Peck W. H., Sinha A. K. and Wei C. S. (2005) 4.4 billion years of crustal maturation: oxygen isotope ratios of magmatic zircon. *Contrib. Mineral. Petrol.* **150**, 561–580.

Vervoort J. D., Patchett P. J., Söderlund U. and Baker M. (2004) Isotopic composition of Yb and the determination of Lu concentrations and Lu/Hf ratios by isotope dilution using MC-ICP-MS. *Geochem. Geophys. Geosyst.* **5**, Q11002.

Veizer J. and Mackenzie F. T. (2003) Evolution of sedimentary rocks. In *Treatise on Geochemistry* (eds. H. D. Holland and K. K. Turekian), Pergamon, Oxford, pp. 369–407.

Wan Y. S., Zhang Y. H., Williams I. S., Liu D. Y., Dong C. Y., Fan R. L., Shi Y. R. and Ma M. Z. (2013) Extreme zircon O isotopic compositions from 3.8 to 2.5 Ga magmatic rocks from the Anshan area, North China Craton. *Chem. Geol.* **352**,

108–124.

Wang W., Cawood P. A., Zhou M. F. and Zhao J. H. (2016) Paleoproterozoic magmatic and metamorphic events link Yangtze to northwest Laurentia in the Nuna supercontinent. *Earth Planet. Sci. Lett.* **433**, 269–279.

Wang W., Zhou M. F., Zhao X. F., Chen W. T. and Yan, D.P. (2014) Late Paleoproterozoic to Mesoproterozoic rift successions in SW China: implication for the Yangtze Block–North Australia–Northwest Laurentia connection in the Columbia supercontinent. *Sediment. Geol.* **309**, 33–47.

Weinberg R. F. and Hasalová P. (2015) Water-fluxed melting of the continental crust: A review. *Lithos* **212–215**, 158–188.

Williams I. S. (1998) U-Th-Pb geochronology by ion microprobe. In *Applications of microanalytical techniques to understanding mineralizing processes* (eds. M. A. McKibben, W. C. Shanks III and W. I. Ridley), Rev. Econ. Geol. pp. 1–35.

Yang X. M., Drayson D. and Polat A. (2019) S-type granites in the western Superior Province: a marker of Archean collision zones. *Can. J. Earth Sci.* **56**, 1409–1436.

Zhao X. F., Zhou M. F., Li J. W., Sun M., Gao J. F., Sun W. H. and Yang J. H. (2010) Late Paleoproterozoic to early Mesoproterozoic Dongchuan Group in Yunnan, SW China: Implications for tectonic evolution of the Yangtze Block. *Precambrian Res.* **182**, 57–69.

Figure Captions

Fig. 1. (A) Tectonic outline of the South China Block. Numbers: 1-Dahongshan Group, 2-Dongchuan Group, 3-Hekou Group. (B) Simplified geologic map of the Cuoke area, southwestern Yangtze Block (after Cui et al., 2019). Samples from outcrop CK01 are A-type granites and from MJC03 probably belong to TTG. Samples from the other outcrops are typical SPGs.

Fig. 2. Representative field photographs of ca. 2.35 Ga SPGs from along Xiaohedi River in the Cuoke area.

Fig. 3. Representative photomicrographs of ca. 2.35 Ga SPGs from along Xiaohedi River in the Cuoke area taken with cross-polarized light. Mineral abbreviations: Pl, plagioclase; Kfs, K-feldspar; Qz, quartz; Bt, biotite; Ms, muscovite.

Fig. 4. Chemical variation diagrams for ca. 2.35 Ga SPGs from along Xiaohedi River in the Cuoke area. (A) A/CNK versus A/NK; (B) CaO/Na_2O versus Al_2O_3/TiO_2 (after Sylvester, 1998); (C) CIPW-normative An-Ab-Or (Barker, 1979); (D) molar $Al_2O_3/(FeO_T + MgO)$ versus molar $CaO/(FeO_T + MgO)$ (after Altherr et al., 2000); (E) CaO/Na_2O versus MgO; (D) Rb/Sr versus Sr (Inger and Harris, 1993). In (C), fields of melts from partial melting experiments are from Weinberg and Hasalová (2015), 1-dehydration melting of tonalite and Bt-Ms schist, 2-H_2O undersaturated melting of dacite/greywacke, 3-H_2O present melting of Bt-Ms schist. Literature data are from Cui

et al. (2019, 2020) and Lu et al. (2021).

Fig. 5. Chondrite-normalized rare earth element (REE) patterns (A) and primitive mantle-normalized trace element diagrams for ca. 2.35 Ga SPGs from along Xiaohedi River in the Cuoke area. Literature data are from Cui et al. (2019, 2020) and Lu et al. (2021). Normalization values are from Sun and McDonough (1989).

Fig. 6. Cathodoluminescent (CL) images of zircon grains from ca. 2.35 Ga SPGs from along Xiaohedi River in the Cuoke area with analytical spots. The green ellipses, red ellipses and big green circles represent the analyzed domains of zircon U-Pb age, O isotope, and Hf isotope, respectively. Numbers near zircon denote spot numbers, U-Pb ages (Ga), and $\varepsilon_{Hf}(t)/\delta^{18}O$ values.

Fig. 7. Concordia plots of SHRIMP isotope data for zircon from ca. 2.35 Ga SPGs from along Xiaohedi River in the Cuoke area.

Fig. 8. Plots of age versus $\varepsilon_{Hf}(t)$ (A) and $\delta^{18}O$ (B) for zircon grains from ca. 2.35 Ga SPGs from along Xiaohedi River in the Cuoke area. Box and whisker plots for zircon $\varepsilon_{Hf}(t)$ and $\delta^{18}O$ values are also shown. Abbreviations: G1, Group 1; G2, Group 2; DZ, Discordant zircon grains. Literature data are from Cui et al. (2019, 2020) and Lu et al. (2021).

Fig. 9. Plot of $\varepsilon_{Hf}(t)$ versus $\delta^{18}O$ for zircon grains from ca. 2.35 Ga SPGs from along Xiaohedi River in the Cuoke area. Inherited zircon cores are not shown. Literature data are from Lu et al. (2021).

Fig. 10. Comparison of zircon $\delta^{18}O$ values of ca. 2.35 Ga SPGs (this study) from along Xiaohedi River in the Cuoke area with global zircon $\delta^{18}O$ values. The variation of atmospheric oxygen relative to the present atmospheric level (PAL, orange curve; Kump, 2008), the maximum $\delta^{18}O$ envelope of shales (pink thick line; Bindeman et al., 2016), and the changes in mean $\Delta^{17}O$ of shales (blue dashed line; Bindeman et al., 2018b; purple dashed thick line; recalculated mean $\Delta^{17}O$ of shales from Spencer et al. (2019) based on data from Bindeman et al. (2018b) by the Pettitt-test) are also shown. The red curve represents the maximum zircon $\delta^{18}O$ envelope of SPGs without inherited zircon. Global zircon compilation (grey dots), including both detrital and igneous zircon is from Spencer et al. (2017) and Partin et al (2014). Only synmagmatic zircon from literature data for SPGs are shown. Published data sources for SPGs are listed in the Supplementary material B.

Supplementary Table Captions

Supplementary Table S1 Major (wt.%) and trace element (ppm) contents of ca. 2.35 Ga SPGs from along Xiaohedi River in the Cuoke area.

Note: A/CNK = molar $Al_2O_3/(CaO + Na_2O + K_2O)$, n and R denote chondrite-normalized value and replicate sample, respectively.

Supplementary Table S2 SHRIMP U–Pb data for zircon from ca. 2.35 Ga SPGs from along Xiaohedi River in the Cuoke area.

Errors are 1-sigma; Pbc and Pb* indicate the common and radiogenic portions, respectively. Common Pb corrected using measured ^{204}Pb. Disc. (%) is percentage discordance defined as [1-($^{206}Pb/^{207}Pb$ age)/($^{206}Pb/^{238}U$ age)]*100

Supplementary Table S3 Zircon O-Hf isotope compositions of ca. 2.35 Ga SPGs from along Xiaohedi River in the Cuoke area.

Note: Age is the weighted mean age for synmagmatic zircon, the single spot $^{207}Pb/^{206}Pb$ age for inherited zircon.

Supplementary Table S4 U-Pb ages of Standard zircon Plešovice.

Supplementary Table S5 Hf isotope compositions of Standard zircon.

Supplementary material A Zircon O-Hf isotope compositions of individual dated samples.

Supplementary material B References for zircon oxygen compositions of SPGs used in Fig. 10.

Figure 1

Click here to access/download;Figure;Fig.1.tif

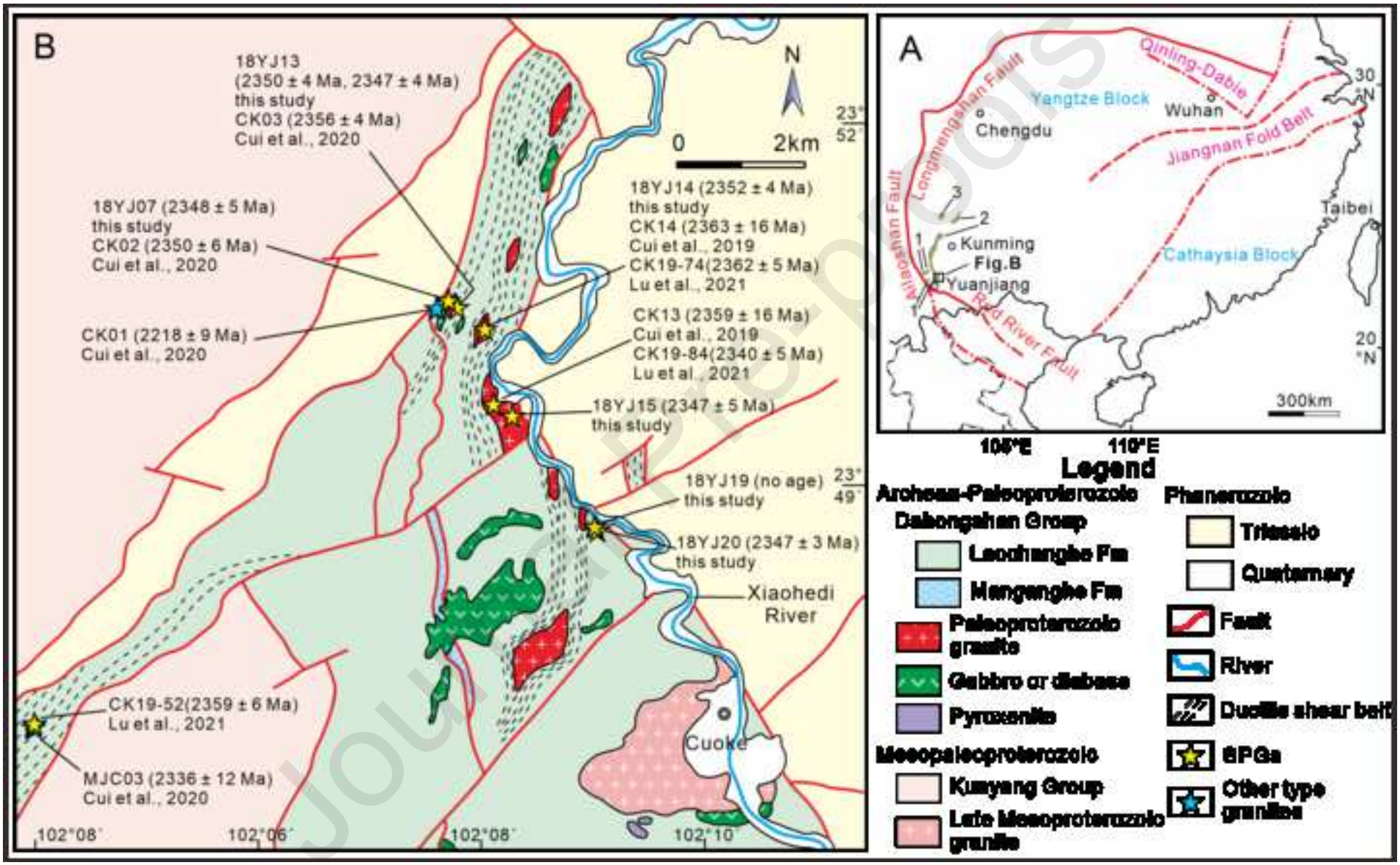

Figure 2

Figure 3

Click here to access/download;Figure;Fig.3.tif

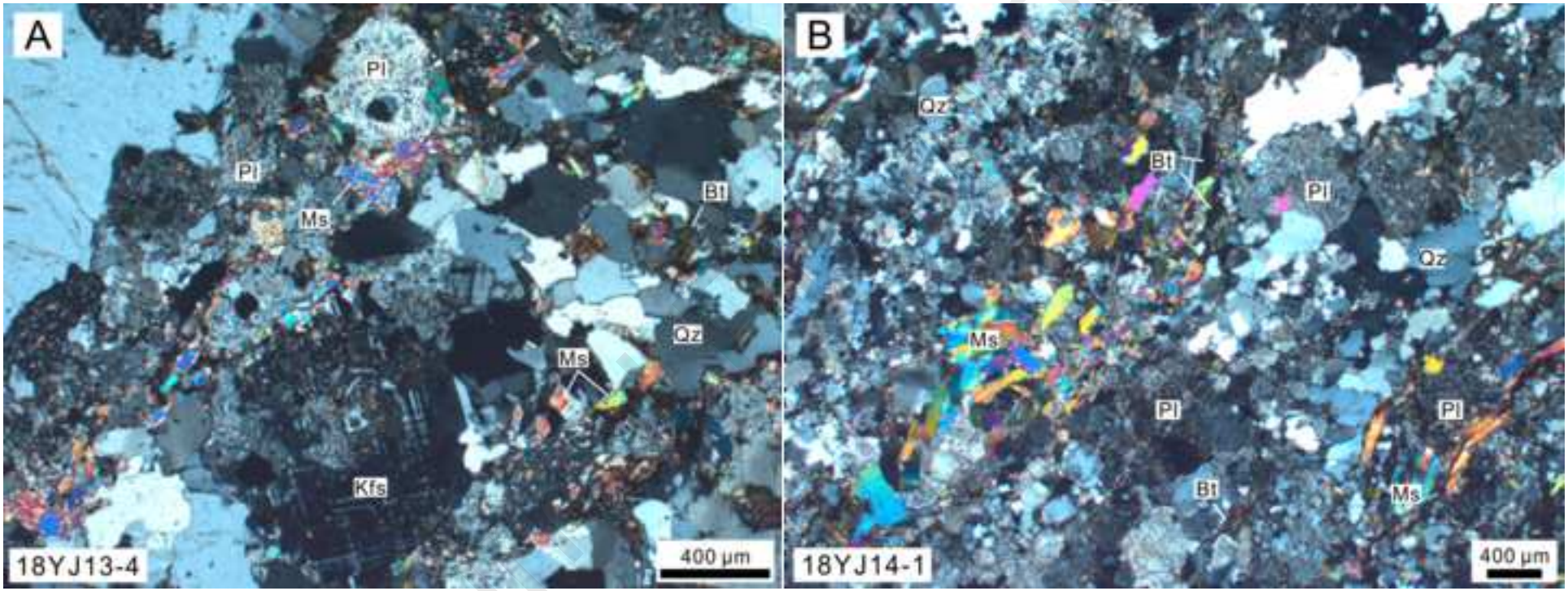

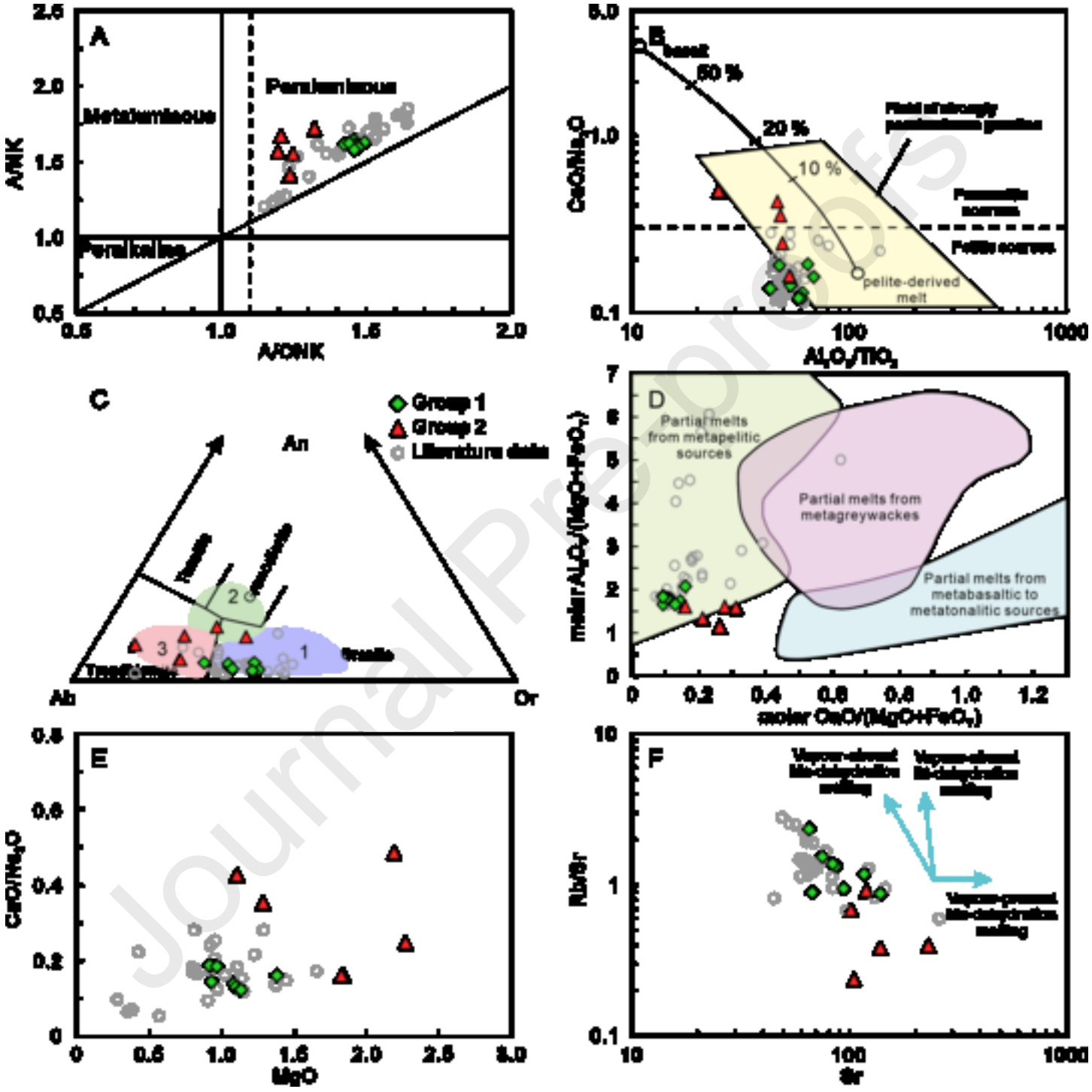

Figure 5

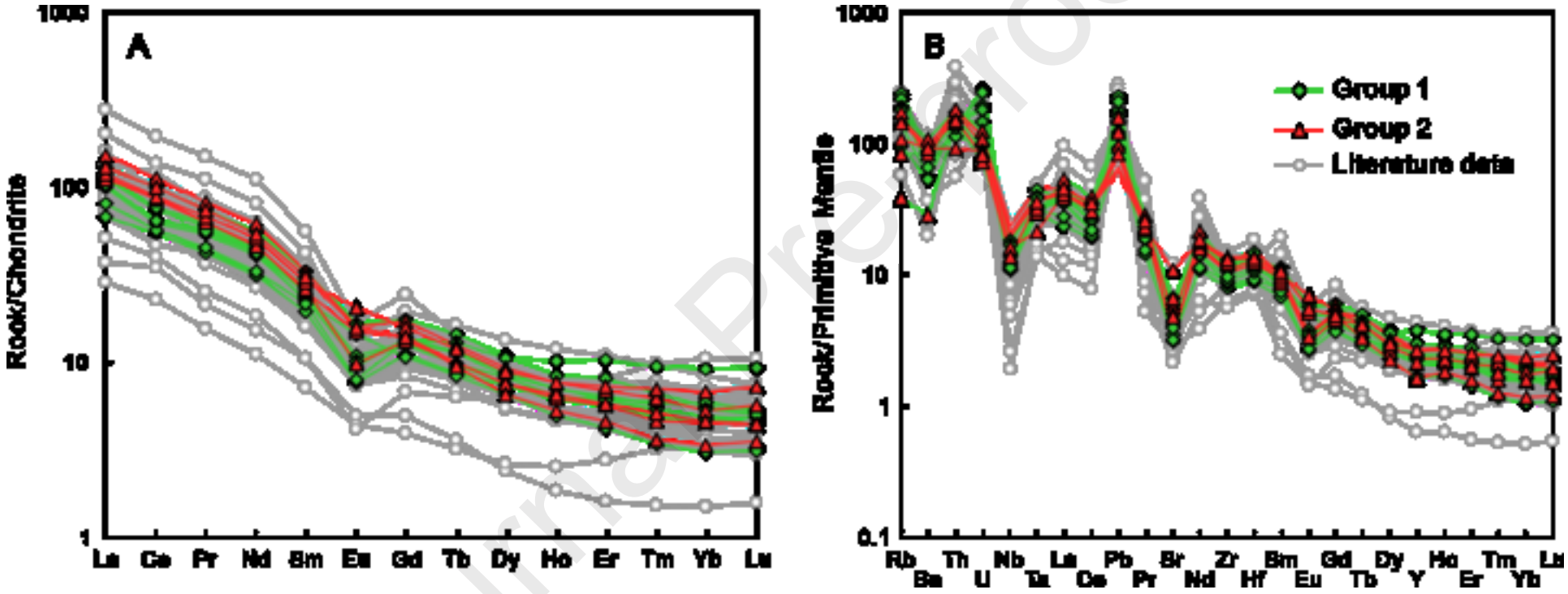

Figure 6

Click here to access/download;Figure;Fig.6.tif

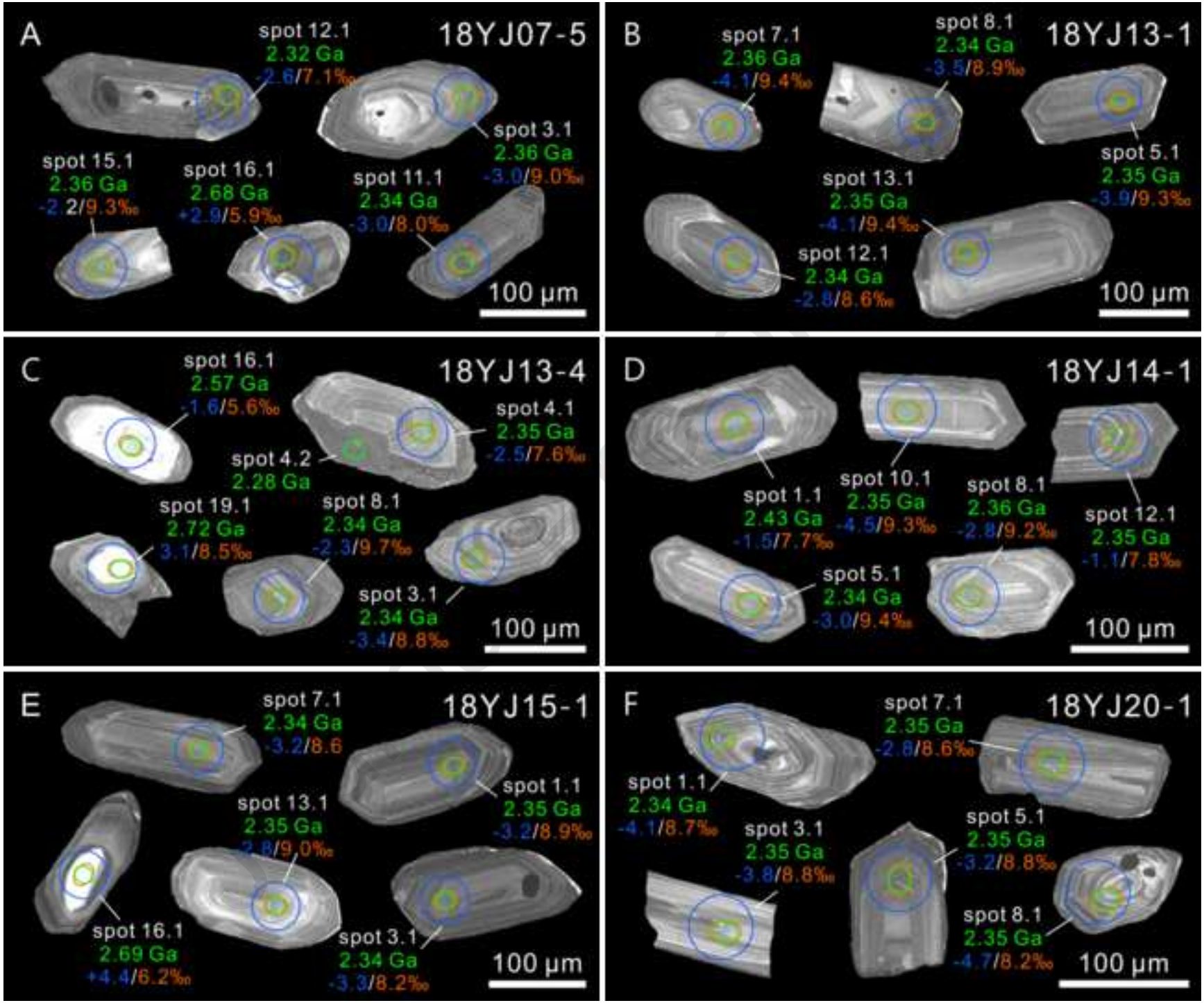

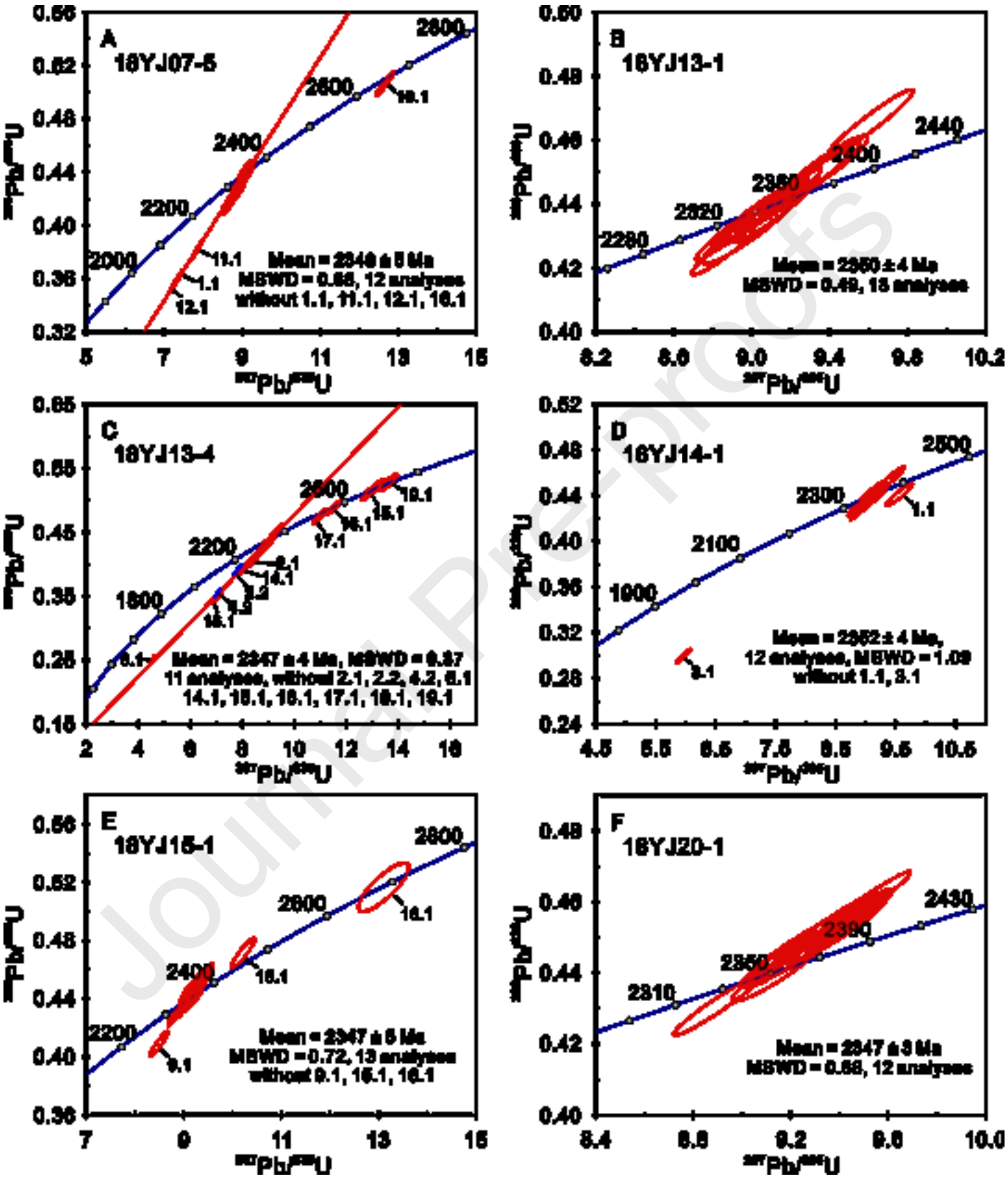

Figure 8

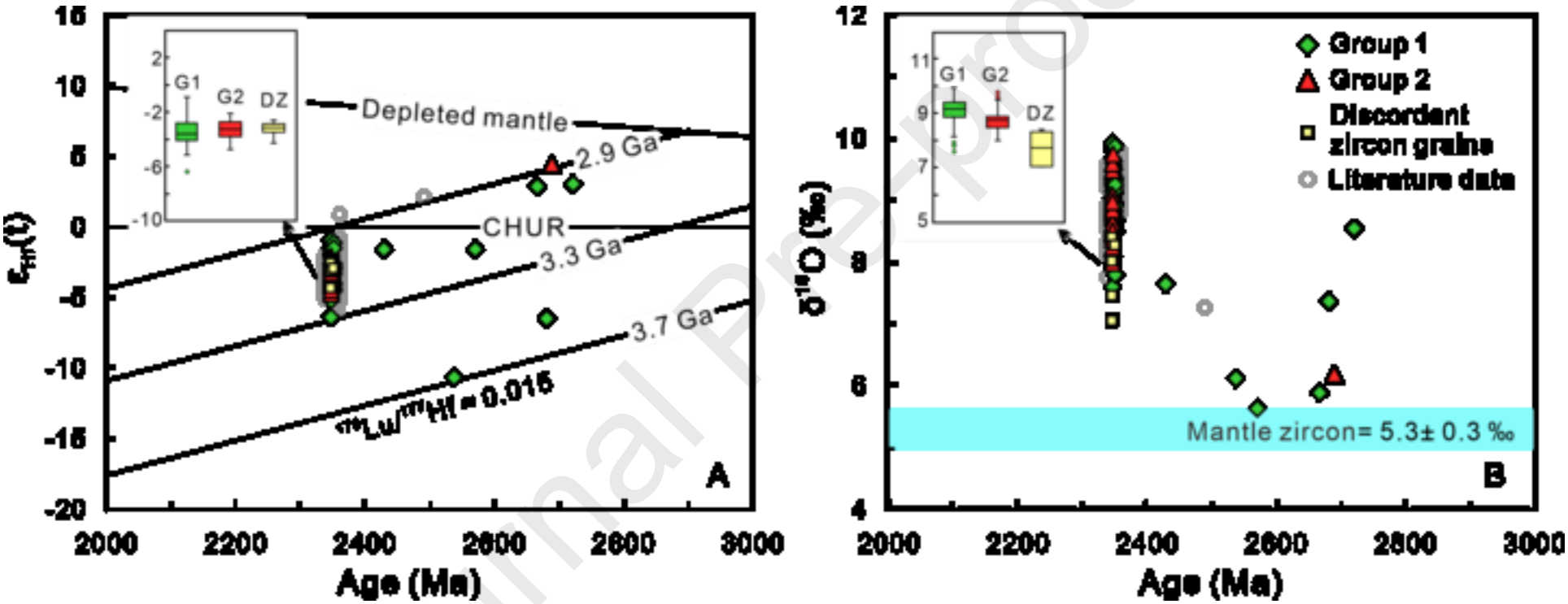

Figure 9

Click here to access/download;Figure;Fig.9.tif

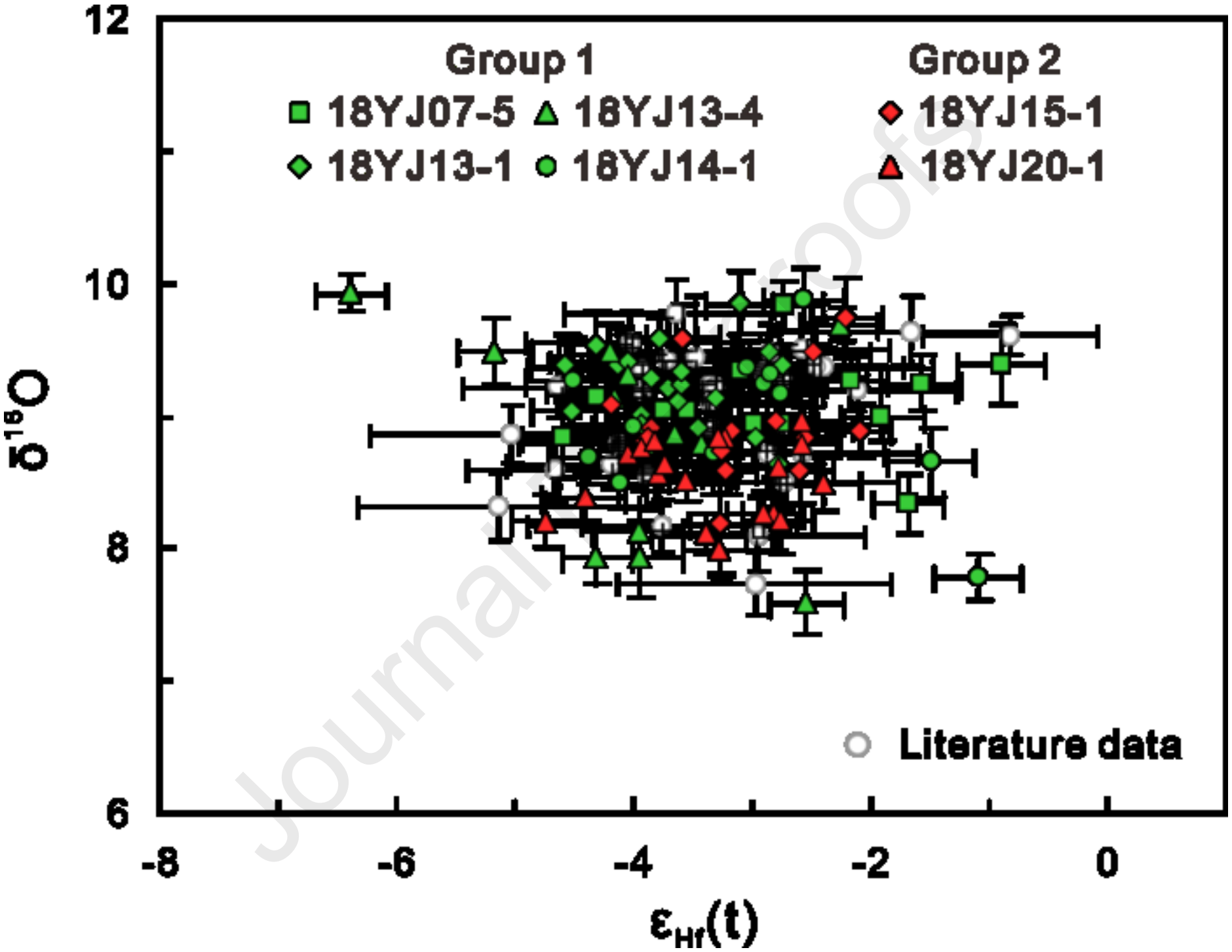

Figure 10